ENVIRONMENTAL RESEARCH
COMMUNICATIONS

INCLUSIVE PUBLISHING TRUSTED SCIENCE

Part of the ENVIRONMENTAL RESEARCH SERIES

PURPOSE-LED PUBLISHING™

PAPER • **OPEN ACCESS**

The changing tropical cyclone hazard in the South-West Indian Ocean and Madagascar regions between 1981–2025

To cite this article: Lionel D Swan and Samantha Hallam 2026 *Environ. Res. Commun.* **8** 115019

View the article online for updates and enhancements.

You may also like

- East–West asymmetry in intensity, duration, frequency of heatwaves over Northern India
Ganaraj Dalal, Shushobhit Chaudhary, Riya Dutta et al.
- Small pelagic fisheries in West Indian Ocean Waters of Sumatera
Hufiadi, H N Yusuf, Baihaqi et al.
- Effect of forming method on the properties of porcelain doped with waste glass
J Ondruška, É B Jakab and M Staník

SmarAct | group

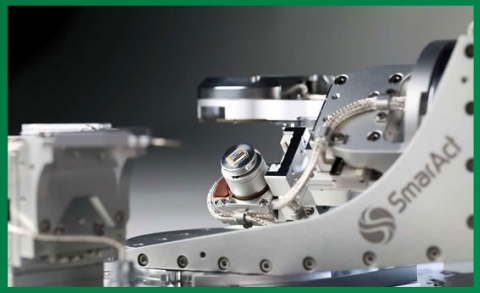
More details and registration

webinar

One sample, many dimensions: prospects for multimodal nanoscale characterization

Explore how precise sample manipulation enables complementary nanoscale techniques to work together on one sample

Live at 2 p.m. GMT/3 p.m. CET,
12 November 2026



This content was downloaded from IP address 149.157.149.136 on 13/11/2026 at 14:14

Environmental Research Communications

Check for updates

OPEN ACCESS

RECEIVED
21 August 2026

REVISED
3 November 2026

ACCEPTED FOR PUBLICATION
6 November 2026

PUBLISHED
13 November 2026

Original content from this work may be used under the terms of the Creative Commons Attribution 4.0 licence.

Any further distribution of this work must maintain attribution to the author(s) and the title of the work, journal citation and DOI.



PAPER

The changing tropical cyclone hazard in the South-West Indian Ocean and Madagascar regions between 1981–2025

Lionel D Swan* and **Samantha Hallam**

Irish Climate Analysis and Research Units (ICARUS), Department of Geography, Maynooth University, Maynooth, Ireland
* Author to whom any correspondence should be addressed.

E-mail: Lionel.swan.2021@mumail.ie and Samantha.hallam@mu.ie

Keywords: tropical cyclone, ocean temperature, ENSO, IOD, MJO, South-West Indian Ocean

Supplementary material for this article is available online

Abstract

Tropical cyclones (TCs) are amongst the most destructive and costly natural hazards that occur around the world and severely affect vulnerable countries such as Madagascar and Mozambique. This study investigates changes in TC hazard in the South-West Indian Ocean (SWIO), the Main TC Region (MTCR) and the Madagascar Region over 45 TC seasons (1981–2025) and examines if there is an association between TC hazard metrics (frequency, maximum sustained wind speed [MSW] and accumulated cyclone energy [ACE] and ocean temperatures or climate indices. Seasonal slopes in frequency and ACE showed no significant values, while MSW increased significantly in all regions (2.8–4.8 knots per decade), strongest in the Madagascar Region. The number of Category 4 TCs per decade was found to have increased significantly in the SWIO. Sea surface temperature (SST) and ocean temperatures at 35 m and 45 m depths warmed significantly in all regions (0.13–0.25 °C per decade), with the subsurface depths warming at a higher rate. The southern oscillation index saw the only significant long-term trend of all the climate indices, but there was little evidence to suggest that any long-term trends in the TC metrics could be explained by any long-term changes in the climate indices. Seasonal associations between TC metrics and climate indices were largely absent, apart from the El Niño–Southern Oscillation indices on TC metrics in the Madagascar Region, where La Niña-like conditions coincided with higher frequency, MSW and ACE. Exploratory analyses suggested higher TC formation and TC-days in Madden–Julian Oscillation phases 2–4 in the SWIO and MTCR. TC hazard in the SWIO and most clearly in the Madagascar Region has increased due to the significant rise in MSWs over the period 1981–2025.

1. Introduction

Tropical Cyclones (TCs) form over tropical and sub-tropical waters as non-frontal organised storm systems, exhibiting a low-pressure central core and spiralling precipitation bands (Doocy *et al* 2013). TCs can form when the following conditions are met; a sea surface temperature (SST) exceeding 26 °C, the convergence of surface winds, the presence of a Coriolis force strong enough to initiate rotation (typically more than 5 degrees from the equator), low sea level pressure ($\leqslant$980 hPa) and the occurrence of weak vertical wind shear (Gray (1968), Emanuel 1999, Tory and Frank 2010, Tory and Dare 2015, Crnivec *et al* 2016). TCs are amongst the most destructive and costly natural disasters that occur around the world (Murakami *et al* 2014). Due to their potential in producing extreme winds, high storm surges, intensive precipitation events, and catastrophic floods, TCs pose a major threat to human life, socioeconomic stability, and biodiversity (Wang and Wu 2004, Bousquet *et al* 2021). Since the beginning of the 20th century, TCs have been responsible for an estimated 1.33 million deaths and have impacted more than 629 million people (Doocy *et al* 2013). Understanding how present day and future TCs might be impacted by Climate Change has become one of greatest concerns for both the World Meteorological Organisation (WMO) and the Intergovernmental Panel on Climate Change (Bousquet

© 2026 The Author(s). Published by IOP Publishing Ltd

et al 2021). Despite extensive scientific research, the influence that climate change has on TCs is heavily debated. This stems from the fact that TC trends over global and regional scales are subject to decadal and interannual variability, largely driven by ocean-atmosphere (OA) modes (Zhao *et al* 2009, Yuan and Cao 2012, Strachan *et al* 2013, Murakami *et al* 2014, Mahala *et al* 2015, Walsh *et al* 2015, Wahiduzzaman *et al* 2022), and none more so than in the South-West Indian Ocean (SWIO) (Vialard *et al* 2008).

The SWIO basin covers the region between 0–40° S and 30–90° E (Bousquet *et al* 2021). The SWIO produces 10%–12% of global TCs, broadly similar to that of the North Atlantic, yet is far less studied (Terry *et al* 2013, WMO 2017, Leroux *et al* 2018). The TC season runs November–April, though off-season storms do occur (Mavume *et al* 2009, Terry *et al* 2013). The basin also contains several fragile countries, suffering from poor infrastructure and the availability of fresh food and water (Bousquet *et al* 2021). From 2000–2020, 39 significant TC severely affected Madagascar, resulting in catastrophic damage and death across the country. Amongst the worst were TC Eline [2000], Gafilo (2004) and Ivan (2008), which saw a combined death toll of over 500 (Rakotoarimanana *et al* 2022). Recent storms such as Batsirai, Emnati (2022) and Freddy (2023) also caused hundreds of deaths and hundreds of millions of dollars in damage (Acaps 2023). Rakotoarimanana *et al* (2022) research highlights an interesting trend in TC activity around Madagascar. Since 2014, there has been a decline in TCs affecting Madagascar, however those that do affect Madagascar have become more intense resulting in more destruction. Between 1980–1993, one singular TC out of the 20 that hit Madagascar brought maximum sustained wind speed (MSW) greater than 200 km h^{-1}. Since then, the number of TCs that have brought winds stronger than 200 km h^{-1} has increased (Republique de Madagascar 2014). Mavume *et al* (2009) published similar findings showing that the number of intense TCs forming in the SWIO had increased from 36 between 1980–1993 to 56 between 1994–2007. Limited research has examined trends in TC accumulated cyclone energy (ACE) in the SWIO. Leroux *et al* (2024) estimated the historical average ACE per storm in this basin to be 8.3 (10^4 $knots^2$) and projected future increases of approximately 36% under a +2 °C scenario and 49% under a +4 °C scenario. Historical analyses indicate that between 1976/1977–1987/1988 and 1988/1989–2007/2008, ACE in the SWIO experienced the largest increase of any Southern Hemisphere basin (Cheung *et al* 2015). However, these studies cover different periods, regions and metrics, so it remains unclear how the hazard from TCs has changed across the SWIO and sub regions within it over the period 1981–2025.

SST plays a crucial role in TC formation and intensification (Miller 1958). Warmer SSTs are often associated with increased TC development and intensity (Vecchi and Soden 2007). As was the case with TC trends, limited papers exist exploring the relationship between SST and TCs within the SWIO. This is despite the fact that the SWIO has seen a sustained decadal rise in SST over the past two decades since the mid-1990s (Li and Su 2021) and an overall increasing trend in SST over the past 69 years (Yan *et al* 2023). From 1952–2007, a ∼0.3 °C rise in SST occurred in the SWIO, and this occurred simultaneously with a frequency decline in TCs and TCs making landfall in the SWIO (Mavume *et al* 2009). On the other hand, an increase in TC intensity was found between 1980–1993 and 1994–2007 and this coincided with a 0.12 °C rise in SST. However, Mavume *et al* (2009) suggests such a small increase in SST cannot fully explain the observed increase in intensity. The ocean mixed layer depth (OMLD), the temperature at specific depths (SOT) and the layer-mean temperature (°C) across a range of depths (OHC) are all thought to play fundamental roles in the formation and intensification of TCs (Wu *et al* 2018). For example, Hallam *et al* (2021) found, in the region around Bermuda, the surface to 50 m layer was the 'expected cyclone induced mixing depth.' Hallam *et al* (2021) highlighted how average ocean temperature across the upper 50 m layer could be used to better predict TC MSW in the region around Bermuda compared to using SST alone. However, few studies have explored whether the same is true in the SWIO.

SST variability in the Indian Ocean, as elsewhere, is partially controlled by OA systems such as the El Niño–Southern Oscillation (ENSO) (Arora *et al* 2016), so their effect on TC trends is of key interest (Lin *et al* 2020). This effect was highlighted by Semgomba *et al* (2025) where they found an increase in TC frequency during El Niño years compared to La Niña years between 1959–2020 in the SWIO (5°–35° S and 30°–90° E). However, Astier *et al* (2015) suggests El Niño conditions push the subtropical jet towards the equator restricting TC activity in the SWIO (0°–30° S and 48°–90° E). Conversely, during La Niña conditions, TC activity is enhanced through a westward moving cyclonic circulation and downwelling Rossby wave. Trends in TCs moving towards southern Madagascar have been linked to a southwards shift of the 26 °C isotherm which is associated with La Niña years (Fitchett and Grab 2014). Burns *et al* (2016) provides more evidence of a negative relationship between TC activity in the SWIO and El Niño events. Another climate index, the Indian Ocean Dipole (IOD), has also be associated with TC trajectory in the Southwestern Indian Ocean, but only when studied alongside ENSO (Ash

and Matyas 2010). Pillay and Fitchett (2019) suggest ENSO has a greater influence on TC activity compared to IOD in the SWIO. The Madden–Julian Oscillation (MJO) is known to influence Indian Ocean weather and climate in several ways (Wang and Rui 1990). One such way is its effect on TC activity. Ho *et al* (2006) found that TC frequency was highest during phase 2–4 of the MJO. In the SIO, MJO was found to influence TC genesis west of 100° E less than east of 100° E (Bessafi and Wheeler 2006). These results were mirrored by Hall *et al* (2001), who found active phases of the MJO were correlated with significantly more TCs in the Australian region (80° E–170° E). Many other studies have conducted similar analysis on MJO and TC activity in a wide variety of regions (Fiji: Chand and Walsh 2010; North Atlantic: Barrett and Leslie 2009, Western North Pacific: Kim *et al* 2008), however a phase-by-phase assessment of TC formation and intensity for the SWIO and sub-regions within it has yet to be carried out.

In this study we aim to address the gaps in the literature evident above in the SWIO using 45 TC seasons (1981–2025). This research differs from previous work in the following ways. (i) perform analysis on the major TC hazard metrics (frequency, MSW and ACE) together; (ii) introduce a data derived main TC region (MTCR) and a Madagascar Region within the SWIO, to provide clarity on where TCs are most active and where they most affect vulnerable populations; (iii) investigate associations between TC metrics and subsurface ocean temperatures and SST; (iv) present long-term trends in climate indices and test whether they can account for the observed TC trends; and finally (v) perform exploratory MJO phase composite analysis for TC formation, TC-days and intensity. The study provides three main results for the SWIO: first, the production of an up-to-date record of TC metrics and their trends (1981–2025); second, assess ocean warming at the surface and at depth, and compute trends in climate indices; and third, evaluate how TC metrics are associated with ocean temperature and climate indices, and determine if any observed change in TC hazard can be linked to them.

2. Data and methods

This study provides a spatial framework for the investigation of TC hazard using three defined regions. The first, the SWIO, spans 0°–40° S and 30°–90° E. This definition is common in prior studies assessing TC activity (Leroux *et al* 2018, Bousquet *et al* 2021, Rakotoarimanana *et al* 2022) and is utilised by the UK Met Office for seasonal TC monitoring (Met Office, n.d.). It also closely resembles the monitoring region of the La Réunion office of Météo-France for TCs in the central and western South Indian Ocean (Terry *et al* 2013).

Within the SWIO, two subregions of interest are defined for further investigation. The first, referred to here as the MTCR, extends from 10° S to 20° S and from 52° E to 90° E. Although not previously defined in the literature, this region was delineated based on a Gaussian kernel density estimate (kernel standard deviation 1.91 ° longitude × 0.85° latitude, Silverman-type rule) of all TC 3 h track points within the SWIO between 1981–2025. The MTCR approximates the main area of the 50% highest-density region (HDR; the smallest region containing 50% of the track density). 81% of the MTCR is covered by the HDR, with the remainder largely situated in the Mozambique Channel. The HDR's location was largely similar when computed using storm-level bootstrap resampling, with a median overlap of 83% with the original HDR (supplementary figure 1). The central corridor of the HDR remained stable under different bandwidths (0.5×–2×, fixed 1°–3°) and under different TC track points tested (only TC with winds $\geqslant$34 kts and one-track point per storm per 1° cell). Additional justification for the latitude bands chosen to represent the MTCR are that they are latitudinally symmetric to the latitude bands of the Main Development Region in the North Atlantic basin (10° N to 20° N) (Goldenberg and Shapiro (1996)).

Although the MTCR captures the climatological centre of TC activity within the SWIO, it contains no major landmasses and therefore holds limited relevance from an impact perspective. To address this, a second subregion—the Madagascar Region—was defined to represent areas where TCs directly affect vulnerable coastal populations. The Madagascar Region spans 10°–30° S and 35°–55° E, encompassing Madagascar and adjacent parts of the Mozambique coastline, where landfalling cyclones frequently result in severe socio-economic impacts. This region also includes a large proportion of the HDR that was not captured by the MTCR as it is situated mostly in the Mozambique Channel, adding further justification for the Madagascar Region's selection.

These three regions are illustrated in figure 1, which also highlights the spatial distribution of TC track density across the SWIO over the past 45 seasons.

Using the data and methods outlined below, an investigation was conducted into the changing TC hazard and its relationship with oceanic and atmospheric variables and indices across the SWIO, MTCR

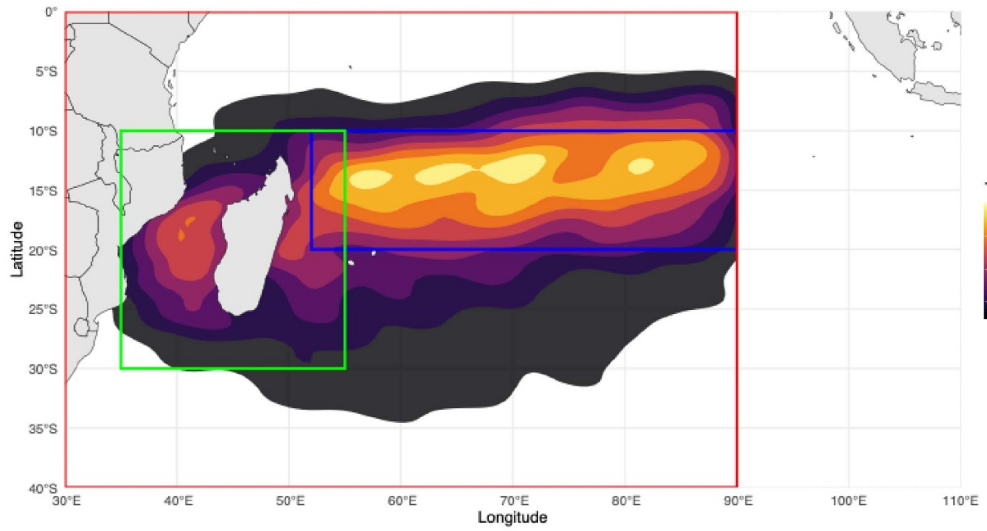


Figure 1. Tropical cyclone (TC) track density across the South-West Indian Ocean (SWIO) over 45 TC Seasons (1981–2025). The three study regions are outlined: the SWIO region (red border: 0°–40° S, 30°–90° E), the *main tropical cyclone region* (blue border: 10°–20° S, 52°–90° E), and the Madagascar Region (green border: 10°–30° S, 35°–55° E). The colour scale represents TC track density.

and Madagascar Region over the last 45 TC seasons from 1981–2025. The annual TC season was defined as November–April as referred to in the literature (Mavume *et al* 2009). Any storms, whether named or unnamed, that occurred outside of the defined TC season were not included in the analysis. All analyses were conducted using either the statistical computing and graphics software R (R 2021) or the programming language Python (Python 2026).

2.1. TC data and metrics

The TC data used in this study was attained from the 3 h Southern Indian subset of the International Best Track Archive for Climate Stewardship (IBTrACS V4.01) (Knapp *et al* 2010, Gahtan *et al* 2024). For frequency analysis, the total number of TCs that formed within or tracked into each of the three study areas were calculated per season and per month. Storms that entered a region only briefly before leaving again are included. Each of the three study regions were assessed separately allowing for the same storm to be counted in multiple regions.

MSW data was calculated using the WMO 10 min and USA agency's 1 min sustained wind measurements (Recorded at height 10 m) included in the IBTrACS dataset. The WMO 10 min values were adjusted to 1 min estimates in order to align with the USA values. This was achieved by applying a 1.12 multiplier as recommended in the IBTrACS Technical Document (Knapp *et al* 2010). MSW for each TC was defined as the peak measurement out of the USA or WMO values. Using each TC's MSW value, the average MSW was then calculated for each season and month. This resulted in each storm contributing just one value towards the average within its given TC season or month. The following equations were used to compute MSW for each individual TC track point (1), storm (2), season (3), and month (4–5):

$$V_{i,t} = \max\left(V_{i,t}^{\mathrm{USA}}, 1.12V_{i,t}^{\mathrm{WMO}}\right) \tag{1}$$

where $V_{i,t}^{\mathrm{USA}}$ and $V_{i,t}^{\mathrm{WMO}}$ are the USA and WMO wind estimates for storm i at track point t. Where only one agency reported a value, that value was used.

For each storm i, MSW was defined as its highest value over all track points:

$$\mathrm{MSW}_i = \max V_{i,t}. \tag{2}$$

The seasonal mean MSWs (MMSWs) is the average of the storm MSW values in season s:

$$\overline{\mathrm{SMSW}}_{\mathrm{s}} = \frac{1}{N_{\mathrm{s}}}\sum_{i=1}^{N_{\mathrm{s}}} \mathrm{MSW}_{i,\mathrm{s}} \tag{3}$$

where s is the season and N_{s} is the number of storms in the season.

For the monthly analysis, each storm's maximum wind within its calendar month was taken:

$$\mathrm{MSW}_{i,\mathrm{m}} = \max V_{i,t,\mathrm{m}} \tag{4}$$

where m is the month

The monthly MMSW is then the average of these values over all storms within a given month:

$$\overline{\mathrm{MMSW}}_{\mathrm{m}} = \frac{1}{N_{\mathrm{m}}} \sum_{i=1}^{N_{\mathrm{m}}} \mathrm{MSW}_{i,\mathrm{m}} \tag{5}$$

where N_m is the number of storms in the month

The MSW values were then converted to intensity categories via the Saffir–Simpson Hurricane Wind Scale.

It was observed during the initial phase of analysis that a significant number of TCs did not have their wind speeds captured by the USA agency. This resulted in many TCs being classified as 'Unknown' (57) when it came to intensity classification due to the lack of MSW values. To mitigate this issue, the IBTrACS WMO agency readings (Originating from either La Réunion agency or Australia's Bureau of Meteorology (BOM) agency) were included as they provided wind speed values for many of the TCs (43) that were not captured by the USA agency. In the case that both La Réunion and BOM winds were recorded, the WMO agency used the La Réunion value.

Sensitivity tests were performed on the MSW and intensity classification results to ensure the IBTRACS recommended conversion factor of 1.12 applied to WMO wind values were robust. The analysis was repeated (i) with the conversion factor varied from 1.00 to 1.14 (Harper *et al* 2010, Barcikowska *et al* 2012), and (ii) using USA winds only and WMO winds only instead of the maximum of the two. Trends were estimated over three periods, 1981–2025, 1990–2025 and 2000–2025 using ordinary least squares (OLS). An effective sample size was estimated from the lag-1 autocorrelation of the residuals. Adjusted p-values and 95% confidence intervals (CIs) were then computed. All three regions were insensitive of the varied conversion factor, and the sign and significance of trends reported in section 3.1.1 remained largely unchanged following the tests. Detailed findings are outlined in section 3.1.1 and supplementary tables 1–4.

ACE, a metric which accounts for TC frequency, intensity and duration, was calculated for each TC using the peak wind speed in kts measurement out of the USA and WMO values for each 3 h track point. The following equation was used to compute ACE for each individual TC:

$$\mathrm{ACE} = \frac{1}{20^4} \sum_{t=1}^{n} V_t^2 \tag{6}$$

where V_t is the peak wind speed in kts out of the USA and WMO values at each 3 h interval.

ACE totals on a seasonal and monthly basis were calculated through the addition of individual TC ACE values. The units of measurement for ACE were 10^4 Knots^2.

2.2. Environmental conditions and climate indices

SST, SOT and OHC were acquired from the Global Ocean Data Assimilation System (GODAS) dataset (Behringer and Xue 2004). SST was defined as the upper most depth (5 m), while the most appropriate depths for SOT was determined by their correlation with MSW, following the approach of Hallam *et al* (2021). The range of depths used to calculate OHC also followed this approach.

Southern oscillation index (SOI), obtained from NOAA (NOAA 2025a), provides monthly sea level pressure differences between Tahiti and Darwin, Australia. Negative (Positive) SOI values typically coincide with El Niño (La Niña) conditions.

Niño 3.4 SST Anomalies and Niño 3 SST Anomalies, attained from NOAA (Huang *et al* 2017, NOAA 2025b), provided monthly SST anomalies from 1982 until present in the Niño 3.4 region (5° N–5° S, 170°–120° W) and Niño 3 region (5° N–5° S, 150°–90° W). Negative (Positive) SST anomalies greater than −0.5 (+0.5) °C are a typical indicator of La Niña (El Niño) conditions.

IOD index, acquired from NASA (Willis *et al* 2025), provided weekly sea surface height (SSH) anomalies from 1993 until present over the area 66° N–66° S, 180° W–180° E. As such analysis was undertaken from 1993 (1994 season) onwards. Negative (Positive) SSH anomalies indicate the occurrence of warm (cold deep) waters in the Eastern Indian Ocean and cold deep (warm) water in the Western Indian Ocean.

MJO index, downloaded from NOAA (Kiladis *et al* 2014), provided daily OMI PC1, OMI PC2 and amplitude values from 1979 to 2022; a detailed description of these variables is available here (NOAA 2026a). MJO phases 1–8 were then computed following the PSL guidance; OMI was converted to the

RMM phase convention (RMM1 = OMI PC2, RMM2 = − OMI PC1) and the phase space was divided into eight 45° sectors as depicted on the schematic found here (NOAA 2026b). A day was only assigned a phase if the amplitude was ⩾1. Days with an amplitude less than 1 were defined as inactive and were used to form the baseline against which the active phases were compared.

2.3. Trend, correlation and composite methods

Long-term trends per decade were estimated for all TC metrics and climate indices using OLS. For the MJO, long-term trends came in the form of the mean amplitude, percentage of active days and number of days within each phase, as averaging the phase arithmetically was not appropriate for a circular variable. The amount of each TC trend that could be associated with each climate index was assessed. The TC metrics (seasonal values) were regressed on to the indices to identify how much each TC metric changes per one unit change of each index. This quantity was then multiplied by the index's own trend providing an implied trend of how much the TC trend would have changed due to the index alone. The delta method was used to produce standard errors (SE) of the implied trend that account for uncertainties in both the slope and index trend.

Seasonal (November–April) and monthly means of the TC metrics and environmental conditions and climate indices (SST, SOT, OHC, SOI, Niño 3 and IOD) were correlated against each other using Pearson correlation.

Finally, specifically for the MJO due to its circular nature, phase-frequency composite was performed by matching the MJO phase and the first track point (formation) of each storm within the study regions at the same date. Counts were then normalised by the climatological number of days in each phase, providing a formations per 100 d variable which was expressed as rate ratios relative to inactive days. TC-days and intense TC-days (MSW of ⩾ 64 kts) were normalised using the same methodology. Mean storm-day maximum wind speed by phase was also computed to assess whether phase had an association with storm intensity. Exact Poisson intervals were used to create CIs for the rate ratios and a SE clustered by storm with $k-1$ degrees of freedom (where k is the number of storms) was used to compute CIs for the mean storm-day maximum wind speed by MJO phase.

Unless stated otherwise above, 95% CIs were computed as $\pm\ t \times$ SE, where SE is either the SE from the OLS trend, the implied trend, or the SE of the correlation coefficient, and t is the 97.5th percentile of Student's t-distribution with $n-2$ degrees of freedom, which approximates ± 2 SE.

3. Results

The following section highlights the key findings of this research. As there are many trends and correlations reported, we distinguish the primary results (seasonal trends and correlations) from the exploratory (monthly trends and correlations and the MJO composite analysis). All findings, trends and correlations were ascertained over the period from 1981 to 2025 unless specified differently in the data and methods section. The results are separated into two parts: section 3.1 (Observed Changes) covers the observed changes in TC hazard (frequency, intensity and ACE), ocean temperature, and climate indices. Section 3.2 (Associations with Ocean Temperature and Climate Indices) investigates the extent to which TC metrics are associated with ocean temperature and climate indices.

3.1. Observed changes

3.1.1. TC hazard

In total, the SWIO (0°–40° S, 30°–90° E) saw 564 storms over the 1981–2025 period. This was on average 12.5 TCs that either formed or tracked into the region per season (November–April). Activity peaked in January (3.4) and February (3.5). Within this broader region, the MTCR (10°–20° S, 52°–90° E) saw 446 storms, averaging at 9.9 TCs per season, also peaking in January (2.57) and February (2.36), while the Madagascar Region (10°–30° S, 35°–55° E) saw 254 storms, averaging 5.6 TCs per season, peaking in January (1.77) and February (2.08). No significant trends in frequency were detected in any of the three regions over the period 1981–2025 (figure 2).

The average TC MSW has increased significantly between 1981–2025 in all three regions (figure 3). In the SWIO, seasonal MSW has increased by 3.91 kts per decade (95% CI 1.57–6.25, $p < 0.01$) (figure 3 (blue)). This is higher than the observed increase in the MTCR of 2.78 kts per decade (95% CI 0.32–5.23, $p = 0.03$) (figure 3 (green)). But the greatest rise was recorded in the Madagascar Region where seasonal average MSW has increased by 4.79 kts per decade (95% CI 1.45–8.14, $p < 0.01$) (figure 3 (red)). In the exploratory monthly analysis, December and February saw increases in MSW in the SWIO (8.93 kts [95% CI 0.88–16.98] and 6.86 kts [95% CI 2.65–11.06]) and MTCR (9.83 kts [95%

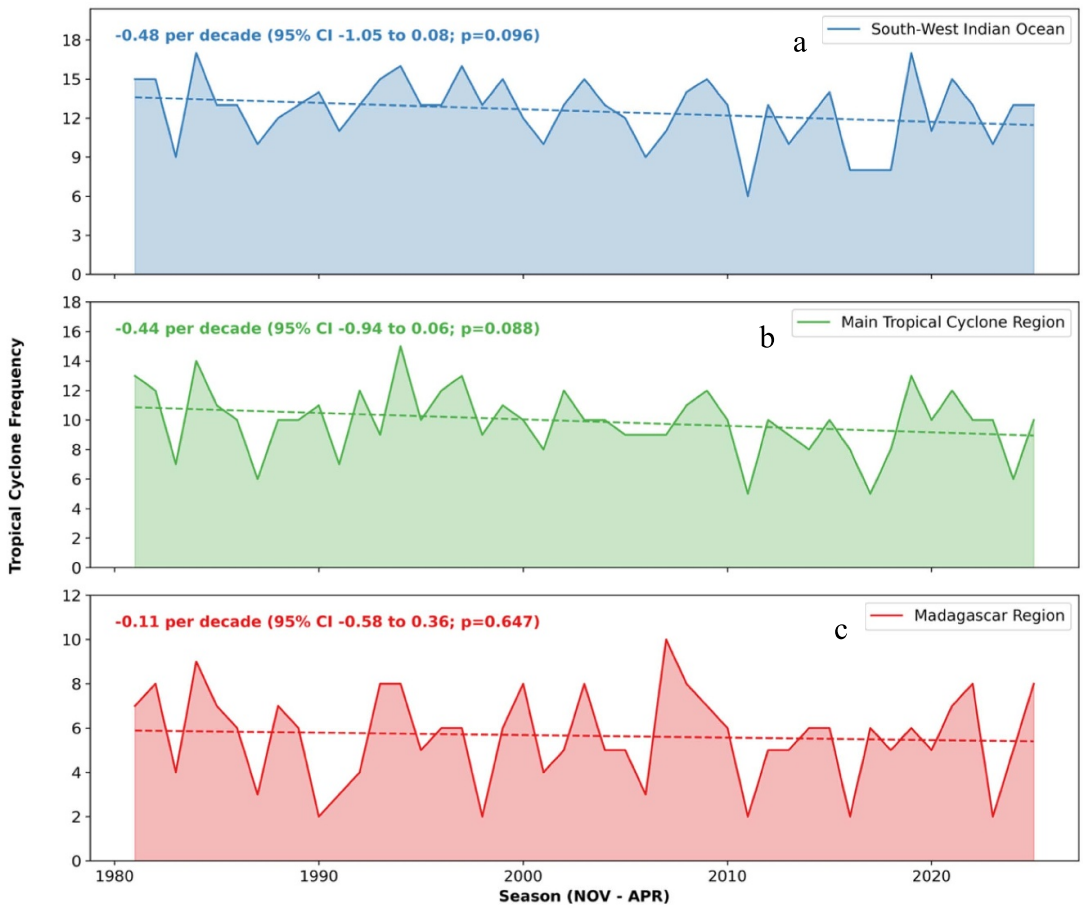


Figure 2. Seasonal tropical cyclone (TC) frequency from 1981 to 2025 for the South-West Indian Ocean (a), Main Tropical Cyclone Region (b), and Madagascar Region (c). Solid lines represent observed seasonal TC counts, while dashed lines indicate linear trends. n = 45.

CI 1.39–18.27] and 7.73 kts [95% CI 1.70–13.76]) respectively. These intervals are much wider than the seasonal intervals and should only be viewed as suggestive.

The overall increase in MSW appears to be linked to an increase in frequency of Category 4 (Cat 4) TCs. The SWIO has seen a significant increase of 0.395 Cat 4 TCs per decade (95% CI 0.03–0.76, $p = 0.04$). However, neither the MTCR nor the Madagascar Region saw significant increases in the number of Cat 4 TCs per decade (0.302, 95% CI −0.01–0.61, $p = 0.06$ and 0.193, 95% CI −0.05–0.44, $p = 0.13$). (supplementary figure 2).

Within the SWIO, results were largely unaffected by the varied conversion factor. The seasonal MMSW changed categories at most in four seasons, with the seasonal MSW trend (3.9 kts per decade) remaining significant following the effective sample size and lag-1 autocorrelation tests (CI 1.6–6.3, $p \leqslant 0.002$). Using USA winds only, the trend was still significant at 3.4 kts per decade (CI 0.8–6.0, $p = 0.01$). The Cat 4 trend remained significant when using only USA winds reporting a +0.41 storms per decade (CI 0.04–0.78, $p = 0.03$). Residual autocorrelation appears to have had negligible effect on significance. Results for 1990–2025 and 2000–2025 were of similar magnitude and sign, with the 1990–2025 MSW trend statistically significant ($p = 0.048$).

Results within the MTCR and Madagascar Regions were also insensitive to the conversion factor, and seasonal MMSW over the entire period remained significant in the Madagascar Region (+4.8 kts per decade, 95% CI 1.4–8.2, $p < 0.01$) and became slightly weaker in the MTCR but remained significant (+2.8 kts per decade, 95% CI 0.1–5.5, $p = 0.04$,) following effective-sample-size adjustment. Seasonal MMSW changed by between 1.7 (MTCR) kts and 2.4 (Madagascar) kts from the lowest to the highest conversion factor. The sign for Cat 4 storms remained positive but was not clearly distinguishable from zero. Results for 1990–2025 and 2000–2025 were again of similar magnitude and sign, but not significant. All sensitivity results can be found in supplementary tables 1–4.

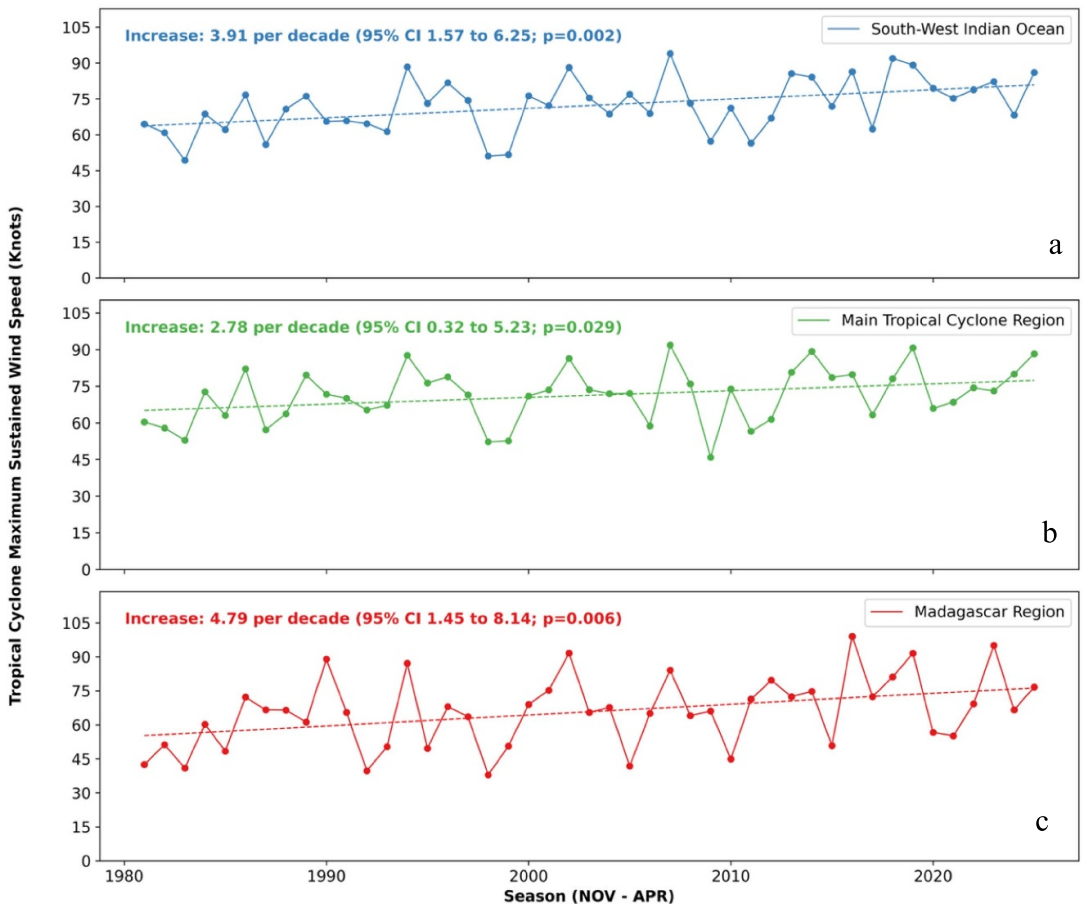


Figure 3. Seasonal tropical cyclone (TC) Maximum Sustained Wind Speed (MSW) from 1981 to 2025 for the South-West Indian Ocean (a), Main Tropical Cyclone Region (b), and Madagascar Region (c). Solid lines represent observed seasonal TC MSW, while dashed lines indicate linear trends n = 45.

The average total ACE per season was 107.4 in the SWIO, 64.46 in the MTCR and 26.69 in the Madagascar Region. The months of January, February and March represented the peak of the season. However no significant seasonal trends in ACE were observed in any of the three regions (supplementary figure 3). As ACE accounts for both frequency and MSW in its calculation—variables which reported opposite slopes, as mentioned in section 3.1.1—it is perhaps not surprising the results are mixed and not significant.

3.1.2. Ocean warming

Analysis of the SST in the SWIO (supplementary figure 4), shows the average seasonal (November–April) SST was 25.15 °C and remained below the 26 °C threshold for TC formation. February (25.89 °C), March (25.95 °C), and April (25.51 °C) were the warmest months. The seasonal SST has increased at a rate of 0.126 °C per decade (95% CI 0.08–0.17, $p < 0.01$), with the exploratory monthly analysis indicating November (0.164 °C per decade, 95% CI 0.12–0.21, $p < 0.01$) and December (0.148 °C per decade, 95% CI 0.10–0.20, $p < 0.01$) having warmed the most.

In contrast, the MTCR exhibited a higher seasonal average SST of 27.6 °C, with peak temperatures in February (28.18 °C), March (28.29 °C), and April (27.92 °C). The SST has increased at a rate of 0.195 °C per decade (95% CI 0.11–0.28, $p < 0.01$) (supplementary figure 4), with exploratory analysis showing November through January warmed around ∼0.225 °C per decade (95% CI 0.13–0.33, $p < 0.01$).

Within the Madagascar Region, the average seasonal SST was similar to the MTCR at 27.24 °C, with the warmest months being January (27.73 °C), February (27.97 °C), and March (27.92 °C). However, the rate of seasonal warming was closer to that of the SWIO, measuring 0.125 °C per decade (95% CI 0.07–0.18, $p < 0.01$), with suggestive increases in the months of November, December, and January being the most prominent ($p < 0.01$) (figure 4). See supplementary table 5 for all SST findings.

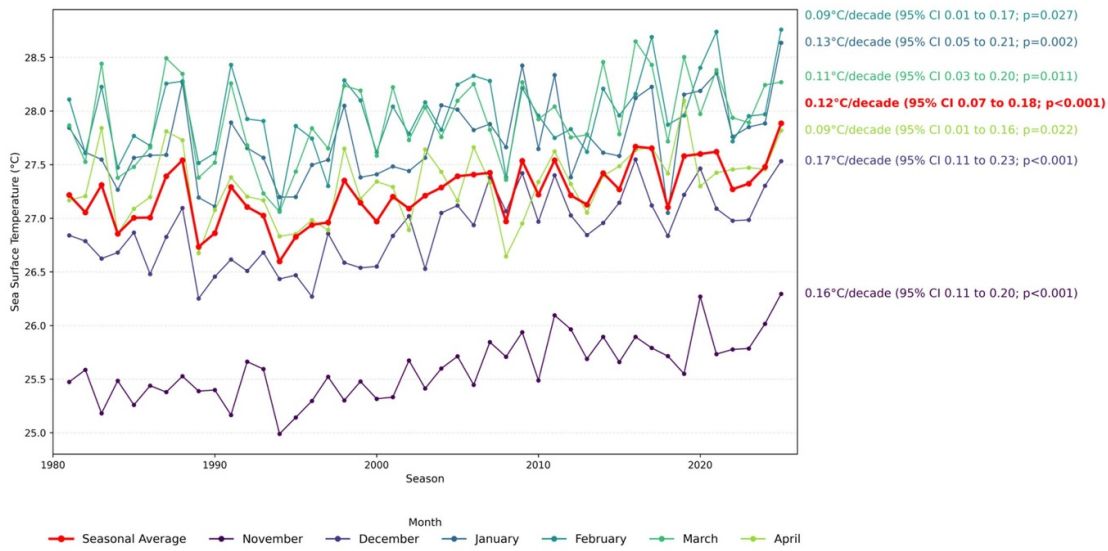


Figure 4. Seasonal and monthly sea surface temperature in the Madagascar Region from 1981–2025. Red line represents the seasonal average, while all other lines represent exploratory monthly averages within the Tropical Cyclone season (November–April). Decadal linear trends are indicated in °C decade^{-1} with 95% CI. $n = 45$.

These results indicate that SST has increased significantly over time in all three regions. While the seasonal warming trend in the Madagascar Region is more similar to the SWIO, its average temperatures are closer to the MTCR. This may be due to the Madagascar Region's more northern location and proximity to the warmer waters of the western Indian Ocean, compared with the SWIO, which extends further south and is affected by cooler subtropical waters. Ocean circulation patterns, including the southward transport of warmer water along the Mozambique Channel, could also help explain the similarity of SST between the Madagascar Region and MTCR despite the warming trend resembling the SWIO. Both the seasonal mean SSTs for the MTCR and Madagascar Regions were above 26 °C, suggesting these regions consistently provide ocean temperature conditions favourable for TC activity. Considering that 79% of all TCs in the SWIO over the 1981–2025 period were found within the MTCR and 45% were found within the Madagascar Region (regions overlap resulting in a shared sum over 100%), the warmest SSTs within the SWIO appear to be where the majority of TCs are found.

Exploratory analysis suggests the early and middle months of the season (November, December, January and February) may be warming at a highest rate and may be extending the length of optimal SST temperatures capable of facilitating the development and intensification of TCs ($\geqslant$ 26 °C).

When assessing which subsurface depths would be the most appropriate to analyse with regard to the TC metrics, the approach of Hallam *et al* (2021) was adopted, whereby the ocean depth was correlated with the MSW to establish the optimum ocean-coupling depth.

Figure 5 highlights that the strongest correlation between MSW and ocean depth is at 45 m in the SWIO and MTCR and 35 m in Madagascar, accordingly these are the chosen depths to analyse here. These depths also coincide with the OMLD, defined as the depth where temperature decreases by 1 °C relative to the surface (Huang *et al* 2018). This was calculated to be 37.2 m in the SWIO, 42.5 m in the MTCR, and 37.5 m in the Madagascar Region. Based on the correlation and OMLD values, the depths of 35 m and 45 m were used for SOT analysis and average temperature across 5–35 m and 5–45 m were used for OHC analyses.

The SOT at 35 m in the SWIO recorded an average seasonal temperature of 24.31 °C, with a significant increase of 0.157 °C per decade (95% CI 0.10–0.21, $p < 0.01$) (figure 6 (red)). Warming was greatest from December to February, ranging between 0.17 °C (95% CI 0.12–0.23, $p < 0.01$) and 0.19 °C per decade (95% CI 0.13–0.26, $p < 0.01$) although this is only suggestive (supplementary table 5). The MTCR warmed more rapidly, at 0.223 °C per decade (95% CI 0.13–0.32, $p < 0.01$), while the Madagascar Region more closely mirrored the SWIO, at 0.155 °C per decade (95% CI 0.10–0.21, $p < 0.01$).

At 45 m, warming rates were higher in the SWIO (0.175 °C per decade, 95% CI 0.11–0.24) and the MTCR (0.246 °C per decade, 95% CI 0.14–0.36) but unchanged in the Madagascar Region (0.155 °C

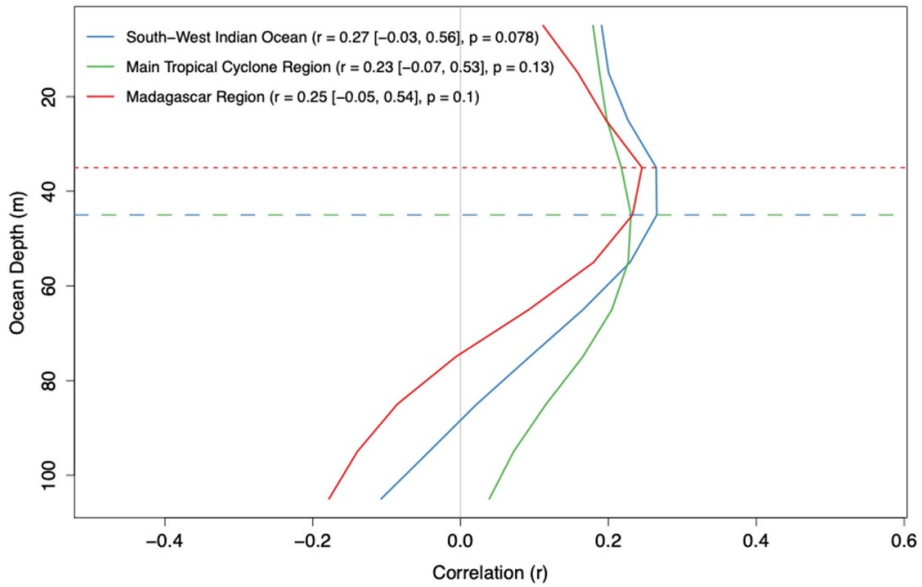


Figure 5. Correlation between maximum sustained wind speed (MSW) and specific ocean temperature (SOT) as a function of depth for the South-West Indian Ocean (SWIO) in blue, the main tropical cyclone region (MTCR) in green, and the Madagascar Region in red. Dashed lines highlight the depth with the strongest correlation in each region. $n = 45$.

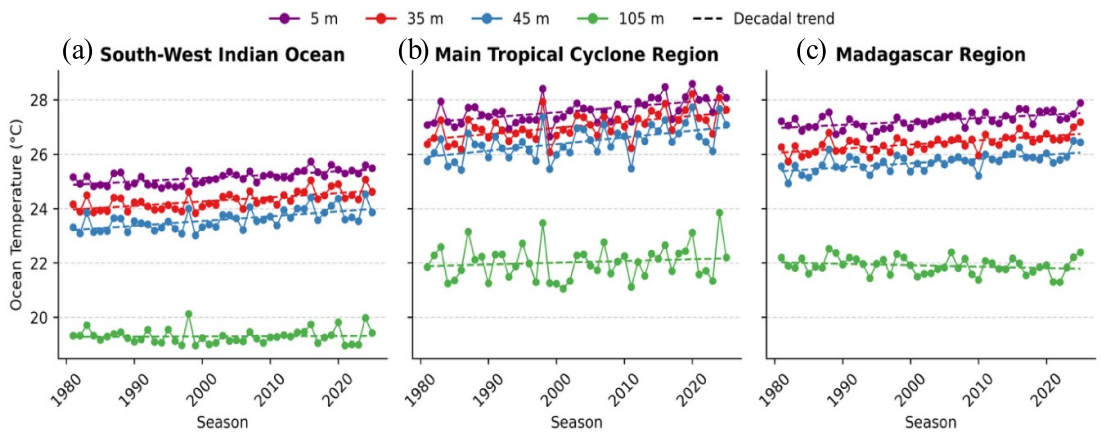


Figure 6. Seasonal average sea surface temperature (5 m) in purple and specific ocean temperatures at 35 m in red, 45 m in blue and 105 m in green across the three study regions—South-West Indian Ocean (a), Main Tropical Cyclone Region (b), and Madagascar Region (c), spanning the 1981–2025 tropical cyclone seasons $n = 45$.

per decade, 95% CI 0.10–0.21) (all $p < 0.01$) (figure 6 (blue)). The exploratory monthly analysis suggests warming peaks between December and March (supplementary table 5). Notably, subsurface warming rates at 35 m and 45 m depths were higher than that of SST (figure 6 (purple)) across all three regions—a key finding of this study.

Temperatures at 105 m were also analysed to assess how conditions vary from the surface, through the OMLD, and below. No significant trends were observed at this depth. However, the Madagascar Region showed a notable temperature rise over the last four seasons (figure 6 (green)).

OHC results (5–35 m, 5–45 m, and 5–105 m) closely resembled the SST and SOT findings. The 5–35 m and 5–45 m layers warmed slightly faster than SST, but slightly slower than SOT at the corresponding 35 m and 45 m depths. The 5–105 m layer also showed significant warming, but at a lower rate compared to the other OHC averages across all three regions. See supplementary table 5 for full OHC results.

Similarly to the SST results, the exploratory monthly analysis suggests the months of November, December, January and February exhibit the greatest rates of rise per decade for each of the SOT depths

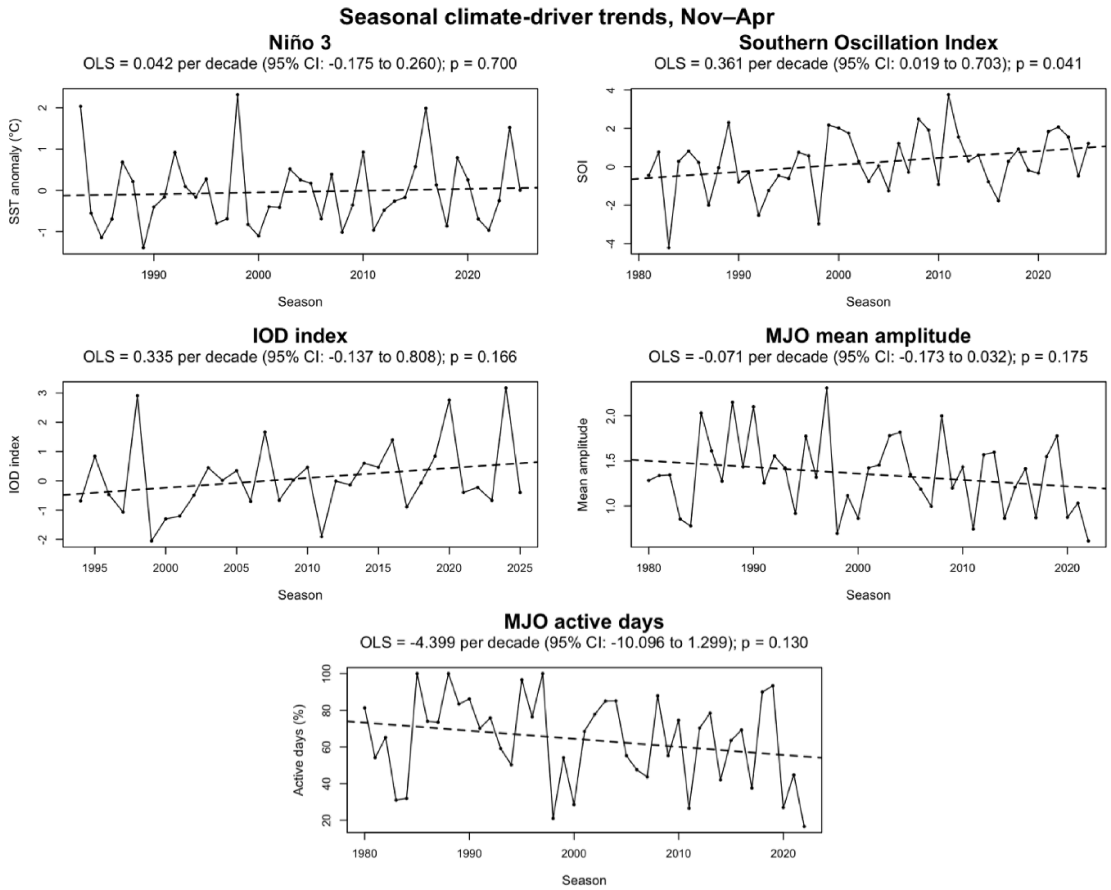


Figure 7. Long-term trends in the climate indices for their seasonal (November–April) means. Record length differs across index: Niño 3 sea surface temperature anomalies (1983–2025), southern oscillation index (1981–2025), Indian Ocean Dipole (1994–2025) and the Madden–Julian Oscillation (1980–2022). Points joined by solid lines show seasonal values and dashed line indicate the slope.

and OHC range of depths. This may suggest that the early to middle months of the season are experiencing the greatest increase in the availability of energy at and below the surface for TC development and intensification.

3.1.3. Long-term trends in climate indices

Long-term seasonal (November–April) values of Niño 3, IOD and MJO (mean amplitude, percentage of active days and percentage of days within each phase) had no significant trends over their respective periods ($p > 0.05$) (figure 7; supplementary table 6). Only the SOI showed a significant trend over time (+0.36 per decade, 95% CI 0.02–0.7, p-value = 0.041). Overall, the long-term trends in TC metrics show little evidence of being significantly driven by long-term trends in the climate indices (supplementary table 7).

3.2. Associations with ocean temperature and climate indices

3.2.1. TC metrics and ocean temperature

SST on a seasonal scale had a negative relationship with TC frequency in the SWIO region exhibiting a significant negative correlation of −0.308 (95% CI −0.60 to −0.02, $p = 0.04$) (figure 8(a)). On a monthly scale, February exhibited a suggestive negative correlation of −0.33 (95% CI −0.64 to −0.02, $p = 0.04$) in the Madagascar Region.

At 35 m and 45 m, the relationship between SOT and TC frequency was negative in the MTCR with a significant relationship at the 45 m depth, with an r value of −0.301 (95% CI −0.59 to −0.01, $p < 0.05$) (figure 8(e)).

For the OHC layer-mean temperature profiles in °C (5–35 m and 5–45 m) only February showed a suggestive negative association at the monthly scale in the Madagascar Region. The 5–105 m OHC profile provided the strongest and most significant seasonal correlations, in the MTCR ($r = -0.309$, 95% CI

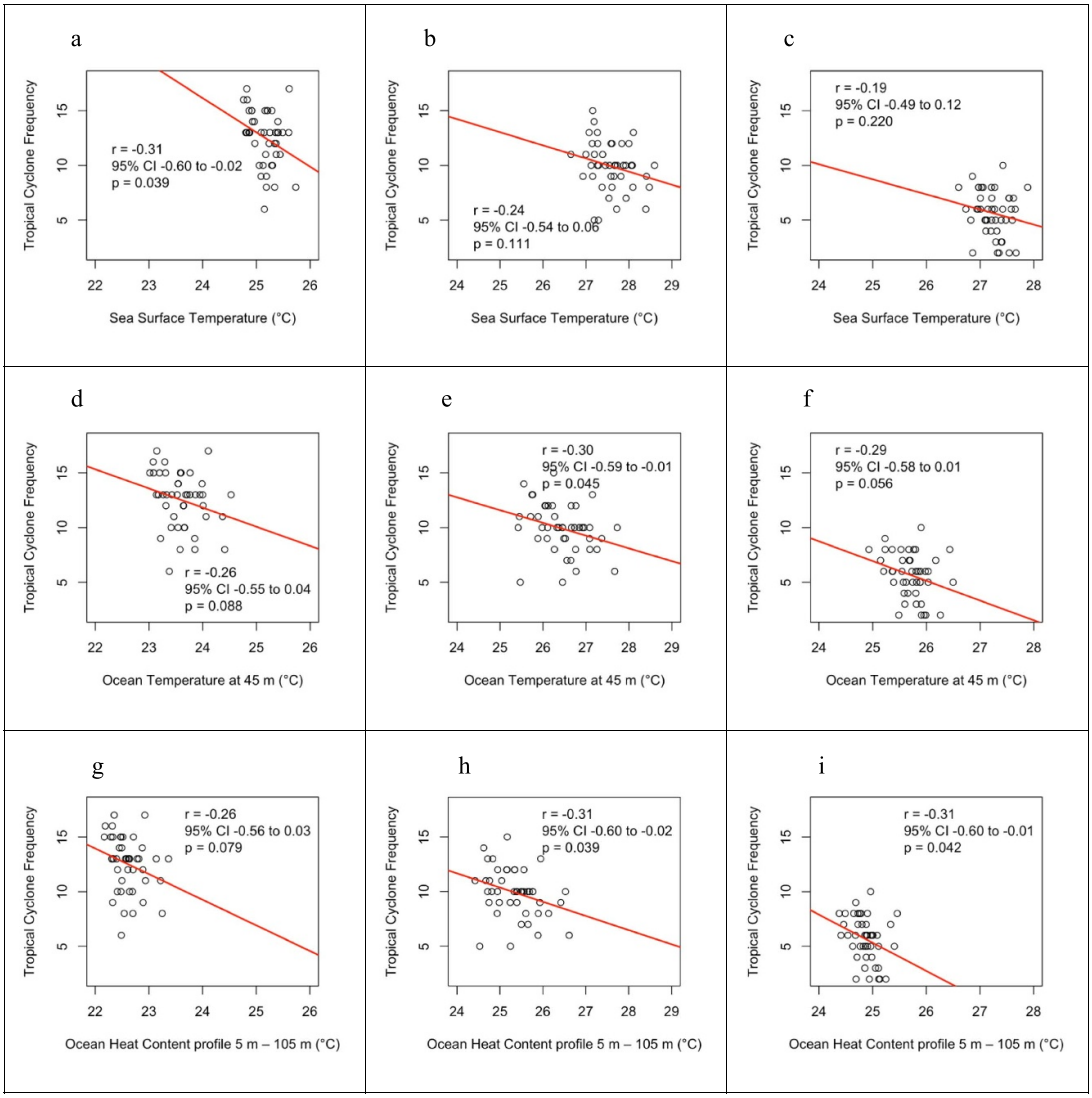


Figure 8. Correlation of seasonal sea surface temperature, specific ocean temperature (45 m) and ocean heat content (5–105 m) with respect to tropical cyclone frequency for the South-West Indian Ocean (a), (d), (g), main tropical cyclone region (b), (e), (h) and Madagascar Region (c), (f), (i) $n = 45$.

−0.60 to −0.02, $p < 0.04$) and the Madagascar Region ($r = -0.305$, 95% CI −0.60 to −0.01, $p = 0.04$) (figures 8(g)–(i)).

There was no significant relationship between seasonal SST and MSW in any region, and only a suggestive association between the month of December and ACE ($r = 0.39$, 95% CI 0.08–0.70, $p = 0.02$) within the MTCR was found.

No significant relationship between SST and ACE was observed on a seasonal basis in any region. A single exploratory association was found between January and ACE ($r = -0.324$, 95% CI −0.62 to −0.03, $p = 0.03$) in the SWIO.

SOT and MSW showed a positive, though not significant, seasonal relationship in all regions. Notably, these correlations were stronger than those found between SST and MSW, suggesting that subsurface temperatures may have a greater association with TC MSW than SST does—a key finding of this study. The 45 m depth had the strongest association with MSW in the SWIO ($r = 0.265$, 95% CI −0.03–0.56, $p = 0.08$) and the MTCR ($r = 0.23$, 95% CI −0.07–0.53, $p = 0.13$), while the 35 m depth had the strongest correlation in the Madagascar Region ($r = 0.245$, 95% CI −0.05–0.54, $p = 0.1$) (figures 9(d)–(f)). Exploratory monthly analysis identified that the MSW during the month of December may have an association at both depths (35 m shown) in the SWIO ($r = 0.421$, 95% CI 0.12–0.72, $p < 0.01$) and MTCR ($r = 0.376$, 95% CI 0.06–0.69, $p = 0.02$) regions.

No significant relationship was observed between SOT and ACE at a seasonal scale, mirroring the SST–ACE findings and further emphasising how the frequency and MSW slopes appear to cancel each other out.

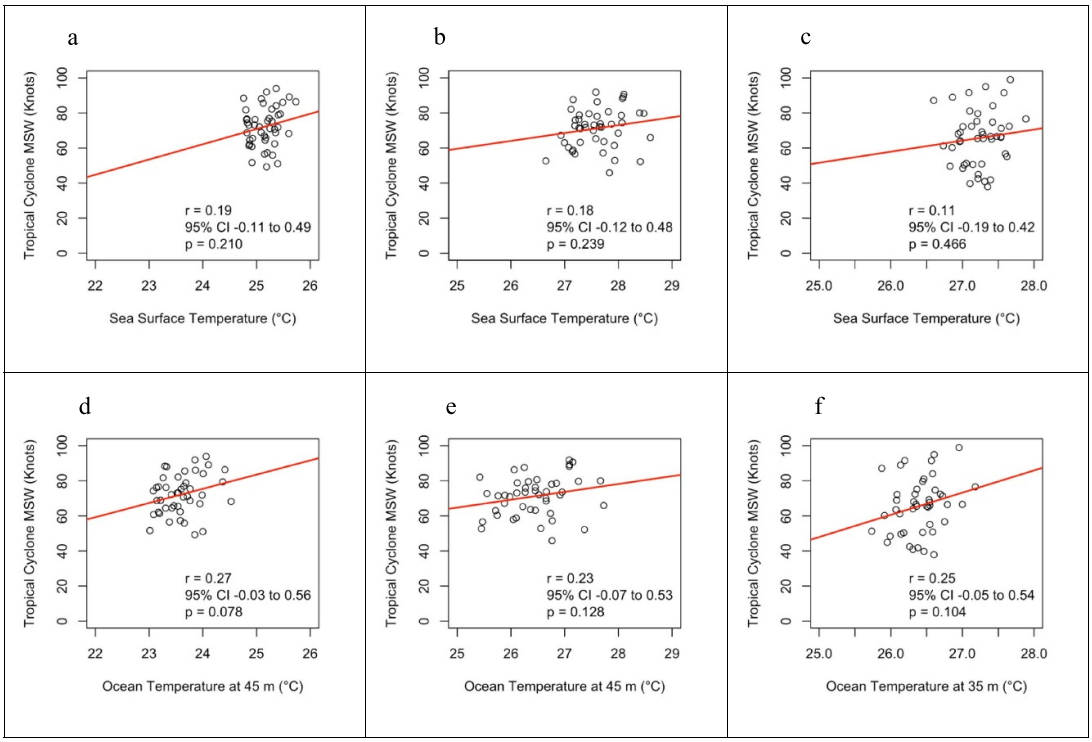


Figure 9. Correlation of seasonal sea surface temperature and specific ocean temperature (35 m/45 m) with respect to tropical cyclone maximum sustained wind for the South-West Indian Ocean (a), (d), Main Tropical Cyclone Region (b), (e) and Madagascar Region (c), (f) $n = 45$.

OHC results for the 5–35 m and 5–45 m mirrored those of the 35 m and 45 m SOT. The month of December exhibited significant relationships with MSW in the SWIO and MTCR, all be it slightly weaker than the individual SOT depths. No statistically significant seasonal or suggestive monthly correlations were found between OHC 5–105 m and MSW or ACE in any region.

See supplementary tables 8 and 9 for all correlation scores between SST, SOT and OHC with respect to the TC metrics.

3.2.2. TC metrics and climate indices (SOI, Niño 3, IOD and MJO)

No significant relationship between SOI and frequency was found at a seasonal level in any region (figure 10(a); supplementary figure 5(a); supplementary figure 6(a)). For seasonal MSW, the relationship with SOI was significant only in the Madagascar Region with a positive correlation ($r = 0.305$, 95% CI 0.01–0.6, $p = 0.04$) (figure 10(b)). The correlation between ACE and SOI in the Madagascar Region was significant ($r = 0.392$, 95% CI 0.11–0.67, $p < 0.01$) (figure 10(c)). The exploratory monthly analysis suggested the months of January and February may be associated with both MSW and ACE across the three regions. See supplementary table 10 for all correlation scores between SOI and TC metrics in all regions.

Niño 3 SST anomalies were found to exhibit an overall stronger and more significant negative relationship with all TC metrics than Niño 3.4 SST anomalies. Therefore, only the Niño 3 SST anomaly results are stated below. A significant seasonal correlation with TC frequency was present in the Madagascar Region ($r = -0.315$, 95% CI -0.61 to -0.02, $p = 0.04$) (figure 10(d)). The month of February showed a suggestive association in the Madagascar Region with frequency ($r = -0.423$, 95% CI -0.73 to -0.12, $p < 0.01$) and ACE ($r = -0.459$, 95% CI -0.75 to -0.16, $p < 0.01$). See supplementary table 10 for all correlation scores between Niño 3 and TC metrics.

The IOD (1994–2025) did not yield any seasonally significant correlations with the TC metrics. Exploratory monthly analysis showed the month of December may be associated with TC frequency in the SWIO ($r = 0.468$, 95% CI 0.11–0.82, $p = 0.01$) and Madagascar Region ($r = 0.705$, 95% CI 0.30–1.00, $p < 0.01$). The month of January may also have a suggestive negative association with MSW in the Madagascar Region ($r = -0.415$, 95% CI -0.78 to -0.05, $p = 0.03$). These associations should be taken cautiously due to their apparent strength when compared to the non-significant seasonal correlations and the reduced sample size as a product of the shorter period of study (1994–2025). See supplementary table 10 for all correlation scores between IOD and TC metrics.

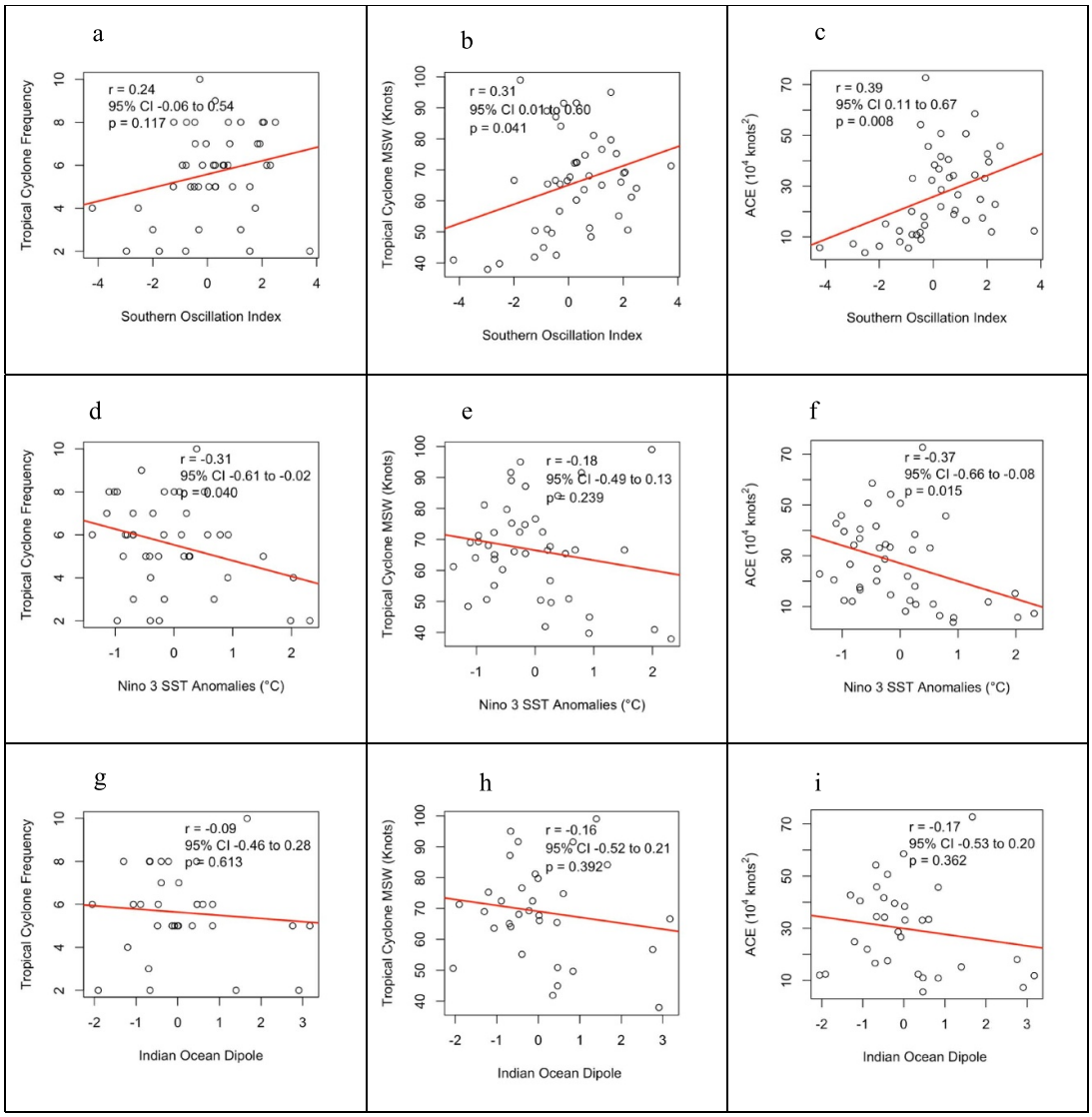


Figure 10. Correlation between seasonally averaged (November–April) climate indices (Southern Oscillation Index, Niño 3 Sea Surface Temperature Anomalies and Indian Ocean Dipole) and tropical cyclone metrics (frequency, maximum sustained wind and accumulated cyclone energy) for the Madagascar Region. n = 45 (Southern Oscillation Index), 43 (Niño 3 SST Anomalies), 32 (Indian Ocean Dipole).

TC count (formation rate) in the SWIO varied with MJO phase (figure 11). There were 9.7 formations per 100 d during phase 3 compared with 6.1 on inactive days (1.58 rate ratio, 95% CI 1.16–2.13, $p = 0.003$). More generally, formations were above inactive days during phases 2 and 4, and below during phases 1, 5 and 8 (0.72–0.85 rate ratio). A normalised chi-squared p-value of 0.002 suggested TC formation differed with MJO phase. A similar pattern was seen in the MTCR with phase 3 rate ratio of 1.59 (95% CI 1.13–2.21, $p = 0.007$). The Madagascar Region also exhibited a similar rate ratio for phase 3 (1.33 rate ratio, 95% CI 0.82–2.08, $p = 0.223$). When grouped, phases 2–4 (in line with Ho *et al* 2006) had a rate ratio of 1.36 times the inactive rate in the SWIO (95% CI 1.09–1.70) and 1.39 times in the MTCR (95% CI 1.08–1.78) but falls to just 1.10 in the Madagascar Region (95% CI 0.78–1.54).

The number of TC-days and intense TC-days displayed a similar pattern with MJO phases in all three regions (figure 11). During phases 3 and 4, there were 83.7 and 86.6 TC-days per 100 d in the SWIO (ratio 1.43–1.48). This was compared to just 58.3 TC-days on inactive days and went as low as 41.7 during phase 8. Intense TC-days followed the same pattern in the SWIO, with 21.4 and 22.8 d per 100 d during phase 3 and 4 compared with only 13.4 during inactive days and 7.3 during phase 8. This equated to a ratio of 1.61 for phase 3 and 1.71 for phase 4. The MTCR and Madagascar Region both exhibited comparable results. Phases 3 and 4 continued to show relatively high numbers of TC-days (MTCR: 44.9–47.3; Madagascar: 21.1–23.9) and intense TC-days (MTCR: 13.8–15.7; Madagascar: 5.2–6.7) compared to inactive days, with ratios typically between 1.2 and 1.8.

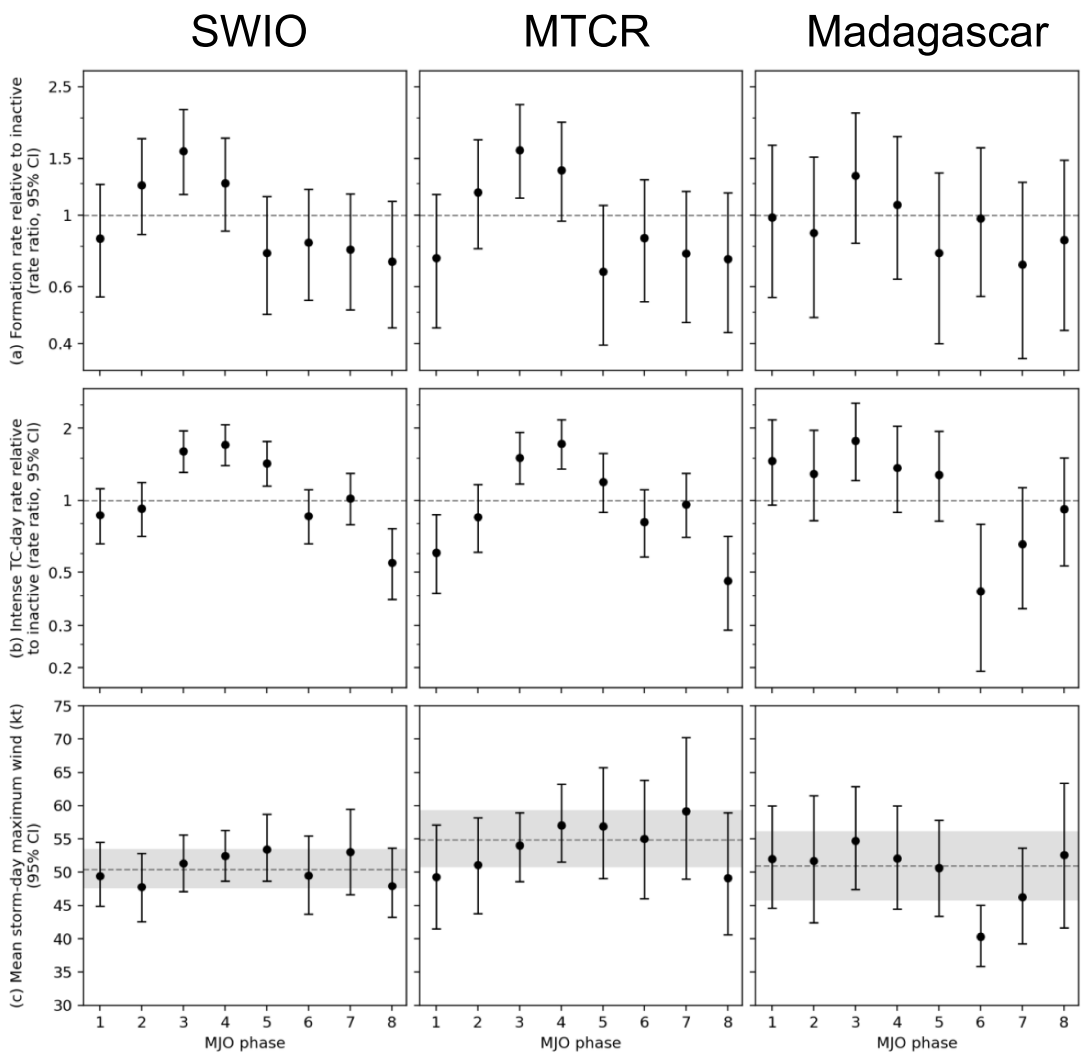


Figure 11. Tropical Cyclone (TC) activity by Madden–Julian Oscillation (MJO) phase in the South-West Indian Ocean (SWIO), Main Tropical Cyclone Region (MTCR) and Madagascar Region. (a) TC formation rate relative to inactive days, (b) rate of intense TC-days (maximum sustained wind speed of $\geqslant$ 64 kts) relative to inactive days, and (c) the mean storm-day maximum wind speed in kts compared to the interval range for inactive days (grey band).

Mean storm-day wind speed on the other hand did not show any clear difference with MJO phase in the SWIO or MTCR. The mean storm-day wind speed for each phase was within the interval range for inactive days (figure 11). This suggests the MJO phases may have an impact on the number of TCs, but not the intensity of them. In the Madagascar Region, mean storm-day wind speed during phase 6 (40.3 kts, 95% CI 35.5–45.1) was lower than on inactive days (50.9 kts, 95% CI 45.7–56.2). However, as this is the only value from 27 comparisons across phases and regions which sits outside the inactive days intervals, this result should be treated cautiously.

Collinearity amongst climate indices were tested using a correlation matrix over the November–April seasonal means. SOI, Niño 3 and IOD were all strongly correlated ($r = 0.73$–0.85) as expected, however variance inflation factors were below the commonly used threshold (5) deemed to determine potential multicollinearity (Vatcheva *et al* 2016). In addition, all indices were tested against the TC metrics independently, reducing concerns over multicollinearity effecting the outcome reported due to not including highly correlated indices inside the same model. As the MJO is a circular variable, phases were not added to the correlation matrix. However, seasonal frequency of each phase (as a percentage of all days) was tested against the other climate indices and were found to be unrelated ($|r| \leqslant 0.25$, $p \geqslant 0.2$).

4. Discussion

4.1. Frequency and intensity

No significant trend in TC frequency was observed in this study in any region. As such, there is no clear sign that there has been a change in the hazard of TCs in the SWIO based purely on the number occurring in the three regions. This is in line with the work of Maue (2011) who demonstrated there was no linear trend in global TC frequency between 1970–2011. However more recent research from Chand *et al* (2022) suggests over a longer period (1900–2012), there is a statistically significant decline in TCs in the South Indian Ocean (0°–90° E). The inconsistencies between TC frequency results between studies is likely a factor of differing temporal and spatial extents.

All three regions have seen a significant increase in the average MSWs experienced over the 1981–2025 period. The most notable increase has occurred in the Madagascar Region (+4.79 kts per decade), while the SWIO (+0.395 Cat 4 s per decade) has seen a significant rise in the number of Cat 4 TCs since the 1981 season. These findings are consistent with observations from previous studies, where an increase in the number of Cat 4+ TCs over the last few decades was found (Webster *et al* 2005, Kossin *et al* 2013). The rising intensity in all three regions reinforce the narrative that the TCs that occur, are stronger and thus more destructive (Elsner *et al* 2008). What is of particular concern is that the highly vulnerable sub-region surrounding Madagascar and Mozambique where TCs cause a serious threat to human life has seen the greatest rise in average MSW but has not seen a significant change in frequency. This suggests the Madagascar Region has experienced an increase in the hazard from TCs over the 1981–2025 period, putting this already underprepared region under even more pressure.

The literature surrounding TC ACE revealed a global decline since the 1970s (Maue 2011, Klotzbach *et al* 2022). However, as discussed in relation to the frequency trends, findings can differ with the period and region studied. No significant seasonal ACE trends were observed in any of the three regions. This is perhaps unsurprising given the absence of a slope in any direction for frequency, with only the slope in MSW being significant. This highlights a possible limitation with the ACE metric, as non-significant slopes in one metric (frequency) may cancel out the impact of another (MSW), resulting in no change in the TC hazard from an ACE perspective, despite a significant increase in intensity.

4.2. Ocean warming

The key findings of this paper highlight how ocean warming is not constrained to the surface but extends downwards through the upper layers of the ocean, potentially impacting TC activity. Significant warming trends at the surface (SST), SOT and across OHC profiles indicate that all three study areas have seen a rise in ocean temperatures over the 1981–2025 period. The inclusion of sub-surface temperature data at specific depths (35 and 45 m) highlighted that these depths have warmed at a similar or even greater rate than at the surface. This is most evident in the MTCR, where SST warmed by +0.195 °C per decade, whereas SOT at 35 m and 45 m exceeded this and warmed by +0.223 °C per decade and +0.246 °C per decade respectively. While considerable research has been conducted on SST and its relation to TC activity (Zhang *et al* 2024), more studies are now including sub-surface temperature data (Lin *et al* 2013, Wu *et al* 2018, Hallam *et al* 2021) due to its importance in fuelling TC intensity via the transfer of latent heat up through the oceans layers (Emanuel 1999). The likely mechanism at play here revolves around the idea that warmer subsurface waters can reduce storm-induced SST cooling, allowing the ocean to remain supplying the storm with energy.

Here, the correlation scores between TC metrics and ocean temperatures show similarities with the above literature but also highlight some key differences. Temperatures at the surface had a weak and non-significant association with MSW. Correlation scores were slightly improved when switching to SOT at 35 m and 45, which exhibited a stronger positive correlation with MSW. The exploratory analysis conducted on the monthly scale showed that the month of December across all ocean variable (SST, SOT and OHC) within the SWIO and MTCR had consistent warming at a higher rate most other months and tended to coincide with the strongest correlations with MSW. This may suggest that the month of December has experienced an increase in its TC hazard within the SWIO and MTCR,

One key difference exists when compared to Hallam *et al* (2021), who found the average temperature across the upper 50 m layer (OHC) exhibited the highest correlation with MSW, whereas here we found the strongest correlation at 45 m and 35 m depths (SOTs). A possible reason for this could be linked to differences in the OMLD between the waters surrounding Bermuda (Hallam *et al* 2021) and the SWIO. This could lead to a difference in the depth at which a TC can draw latent heat up from between the two regions. However, both studies agree that subsurface temperatures have a greater association with TC intensity than with the surface alone.

The correlation scores found between TC frequency and ocean temperatures adds further insight into the complex relationship between TC metrics and ocean temperatures. As all three regions exhibited a negative association with TC frequency for either SST, SOT or OHC, the narrative that increasing ocean temperatures are associated with changes in atmospheric conditions (e.g. vertical wind shear and moisture levels in the atmosphere) in ways that inhibit TC activity (Yoshida *et al* 2017) is potentially evident in this study. It is important to highlight that this association has been observed in the Southern Indian Ocean in other studies (Webster *et al* 2005, Hallam 2021). These studies also affirm the importance of the 26 °C threshold for TC formation, which highlights an apparent contradiction in our results: the seasonal mean SST in the SWIO was below 26 °C and yet TCs form and intensify throughout the season. This is not unheard of, a global study performed by McTaggart-Cowan *et al* (2013) found that 16% of TCs formed in waters below 26 °C. The cooler waters situated along the southern boundary of the SWIO likely contributed to lowering the mean SST, and it is clear from figure 1 that TCs do not tend to form or track into these areas, with 79% of all SWIO TCs occurring within the MTCR where seasonal mean SST are above 26 °C. Furthermore, even with 26 °C or above SSTs, TCs may not form or intensify due to the influence of the other atmospheric factors mentioned above, making predicting future changes in the hazard of TCs a difficult task.

4.3. Role of climate modes: ENSO, IOD, and MJO

This study provides evidence that large-scale climatic modes have varying levels of association with TC activity in the SWIO, MTCR and Madagascar Region between 1981–2025. Niño 3 SST anomalies (key indicator of ENSO conditions) were correlated with TC frequency and ACE between 1983–2025. Positive values of Niño 3 (typical of El Niño conditions) had a significant negative relationship with TC frequency ($r = -0.315$ $p = 0.04$) and ACE ($r = -0.37$ $p = 0.01$) in the Madagascar Region. This suggests that elevated SST in the Niño 3 region during El Niño events could be associated with changes in key atmospheric conditions responsible for TC development in the SWIO. These findings support those from Astier *et al* (2015) and Burns *et al* (2016) but oppose those from Semgomba *et al* (2025). A potential reason for this stems from the difference in study period examined. Semgomba *et al* (2025) analysed years from 1959–2020, including data from the pre satellite era which has been known to be less robust than the post satellite era and could potentially add biases into the findings (Knaff *et al* 2010).

The SOI, another key indicator of ENSO conditions, showed a noteworthy relationship with MSW and ACE between 1981–2025. During La Niña conditions (positive SOI values) MSW and ACE were typically higher. This was particularly evident in the Madagascar Region which saw significant correlation scores for both MSW ($r = 0.305$) and ACE ($r = 0.392$). These findings suggest that during La Niña events, conditions for TC intensification are elevated, especially surrounding the waters of Madagascar and Mozambique. This could be linked to the findings of Fitchett and Grab (2014) who found a shift in the 26 °C isotherm further south during La Niña years which would result in warmer waters and thus more energy for TC intensification surrounding the Madagascar Region.

The IOD exhibited a mixed relationship with TC metrics over the 1994–2025 period. No statistically significant correlations were found on a seasonal scale suggests the IOD has little to no association with TC activity at that scale. This mirrors the findings of Pillay and Fitchett (2019) who found ENSO to have a greater influence on TC activity compared to the IOD.

The exploratory MJO phase composite analysis suggests certain TC variables may vary with phase. In the SWIO and MTCR, the number of storms (formations) was around 1.6 times more frequent during phase 3 compared to inactive days, and was less frequent during phases 1, 5 and 8. By grouping phases 2–4 together to allow for closer comparison with Ho *et al* (2006), and it further suggests the association between phases and TC numbers, with formation rates of 1.36 (95% CI 1.09–1.70) and 1.39(95% CI 1.08–1.78) times the inactive rate for the SWIO and MTCR respectively. These grouped findings align well with Ho *et al* (2006) who found higher frequency of TCs occurred during phases 2–4 of the MJO.

The percentage of TC-days and intense TC-days also showed evidence that suggest they may be associated with MJO phases in the three regions. During phase 3 and 4, TC-days and intense TC-days were higher (44%–49% for TC-days, and 60%–70% for intense TC-days) compared to inactive days of the MJO in the SWIO. The largest increase was seen during phase 3 for the number of intense TC-days within the Madagascar Region (77% increase compared to inactive days)., Interestingly, however, mean storm-day wind speed did not appear to be associated with MJO phase, with only one phase—region association (phase 6—Madagascar) out of the total 27 comparisons (nine phases including inactive periods and three regions) recording a value outside of the inactive range.

As each MJO phase marks the location of its convective envelope, with phases 2–4 situating over the equatorial Indian Ocean and Maritime Continent (Bureau of Meteorology 2026), the associated reduced vertical wind shear, increased atmospheric moisture levels and stronger low-level cyclonic vorticity over

this region (Klotzbach 2014) might help explain the higher number of TC formations and higher number of intense TC-days during these phases.

This study highlights the multi-faceted nature of TC variability in the SWIO, MTCR and Madagascar Region. The key findings emphasise how no single variable can fully explain the trends observed in TC frequency, intensity and ACE between 1981–2025. Mixed statistical significance and contrasting trends and correlations between regions highlight the importance of regionalisation and the inclusion of multiple variables to best capture TC dynamics. By incorporating various climate modes and ocean temperature variables into studies and forecasting models, vulnerable regions around the world such a Madagascar and Mozambique are likely to benefit from improved early warning systems and better risk mitigation strategies.

4.4. Uncertainties, limitations, implications, and future work

This study has shown strong evidence of a change in TC hazard within the SWIO and Madagascar Region in particular. However, several potential uncertainties and limitations must be acknowledged. The IBTrACS dataset—while highly detailed, contains missing values and inconsistencies with regards to wind speed measurements between agencies. This was mitigated by standardising wind speed measurements across the USA and WMO agencies, providing a more consistent sample of measurements across the study period. A second potential limitation comes from the coarse temporal resolution used to assess climate modes, in particular ENSO, IOD and MJO. By averaging these indices over a seasonal or monthly scale, finer day to day changes or extremes that could be important for TC activity might have been masked. Future work should look at employing singular event-based analysis, where observation of SST, SOT, OHC and climate modes are reviewed in the days surrounding individual TCs. This analysis would offer a higher temporal resolution and might uncover more key triggers of TC activity.

The key findings in this study carry substantial weight for potentially improving risk assessment and planning in the SWIO and Madagascar Regions. A clear change towards an increase in TC hazard has been observed, fuelled by the increase in intensity, which may to be associated with the significant increase in ocean temperatures observed, within the Madagascar Region. This highlights an increased threat to the vulnerable countries of Madagascar and Mozambique and emphasises the need for greater attention and investment into the region in order to help mitigate future TCs disasters. This study and future research in this area can promote development of early warning systems and tools, as demonstrated by Hallam *et al* (2026) in the deployment of the TOPIM model across the Caribbean, to better prepare and protect the vulnerable regions affected by TCs around the globe.

5. Conclusion

Over the 1981–2025 seasons, TC frequency showed no significant trend in the SWIO, MTCR or Madagascar Region. In contrast, MMSW increased significantly in all three regions, by 3.9 (SWIO), 2.8 (MTCR) and 4.8 (Madagascar Region) knots per decade, and Category 4 storms became more frequent in the SWIO. ACE showed no significant trend. The MSW trends were robust to the wind conversion factor but were mostly not significant over the shorter 1990–2025 and 2000–2025, emphasising the importance of studies over a sufficiently long period to detect trends over interannual variability. Together, these results indicate an increase in TC hazard across the SWIO region, largest in the Madagascar Region.

Ocean temperatures warmed significantly at the surface and at 35 m and 45 m depths in all regions (0.13–0.25 °C per decade). Subsurface depths were found to be warming at a higher rate than the surface. Seasonal correlations between ocean temperature and TC metrics were weak–moderate, negative for frequency and positive for MSW. Correlations with MSW were highest at 35–45 m suggesting ocean temperatures at these depths may be associated more with MSW than SST is.

Long-term trends in the climate indices were absent except for the SOI. There was little evidence to suggest any long-term changes in ENSO, the IOD or the MJO could account for the observed TC trends. Seasonal associations with ENSO indices were largely confined to the Madagascar Region, where La Niña-like conditions coincided with higher MSW and ACE (SOI, Niño 3) and with higher frequency (Niño 3). The IOD showed no seasonal association. Exploratory analyses suggested higher TC formation rates in MJO phases 2–4 in the SWIO and MTCR, and higher TC-days and intense TC-days in phases 3 and 4 in all regions. However, mean storm-day wind speed showed no clear association with phase, suggesting phase may be linked to changes in TC frequency but not intensity.

This study's findings emphasise the need for greater attention and investment in future research, early warning systems and mitigation strategies within the SWIO and Madagascar Region as TC hazard increases. The vulnerable countries of Madagascar and Mozambique have seen the greatest rise in TC hazard and are potentially going to experience even great levels of devastation from TCs as the planet continues to warm.

Acknowledgments

The analysis presented in this paper was initially conducted as part of the first author's MSc thesis at Maynooth University. The first author would like to thank Professor Conor Murphy, course coordinator of the Climate Change Masters, for their guidance and support throughout this work.

Data availability statement

International best track archive for climate stewardship (IBTrACS). Version (ibtracs.SI.list.v04r01.csv). Accessed on 29 September 2026 at www.ncei.noaa.gov/data/international-best-track-archive-for-climate-stewardship-ibtracs/v04r01/access/csv/.

NCEP Global Ocean Data Assimilation System (GODAS). Accessed on 29 September 2026 at https://ftp.cpc.ncep.noaa.gov/godas/monthly/.

Southern Oscillation Index (SOI). Accessed on 29 September 2026 at www.ncei.noaa.gov/access/monitoring/enso/soi.

Niño Regions Sea Surface Temperatures (Niño 3 and Niño 3.4 Sea Surface Temperature Anomalies). Accessed on 29 September 2026 at www.ncei.noaa.gov/access/monitoring/enso/sst.

NASA Sea Surface Height Indian Ocean Dipole Indicator (IOD).V1.20250508. Accessed on 29 September 2026 at https://podaac.jpl.nasa.gov/dataset/NASA_SSH_IOD_INDICATOR.

The Original OLR Madden-Julian Oscillation Index (MJO). Accessed on 29 September 2026 at https://psl.noaa.gov/mjo/mjoindex/.

R Studio (version 2025.05.1+513) and Python (version 3.13.7) were used to run the entirety of the analysis. An OLS-trend function was created in R, while a simple Pearsons correlation was performed using the cor.test function in R. The Kernel Density Estimate shown in figure 1 was created using the MASS::kde2d() function and the stat_density2() using their default parameters in R. A function was created in R to compute the Madden-Julian Oscillation phases based on the pc1, pc2 and amplitude data values.

All data that support the findings of this study are included within the article (and any supplementary files).

Supplementary Material available at https://doi.org/10.1088/2515-7620/aebf32/data1.

Funding declaration

LS is supported by the WASITUS project funded by the EPA and Met Éireann (Grant number: 2024-CE-1265).

SH was supported by the TOPIM project. The TOPIM project is part of Ireland's 'Our shared Ocean Programme' and is funded by the Department of Foreign Affairs through Ireland's development cooperation programme, Irish Aid, administered and managed by the Marine Institute on behalf of Irish Aid. Grant Agreement Number OSO/22/PA/001. SH was also funded by ObsSea4Clim. ObsSea4Clim 'Ocean observations and indicators for climate and assessments' is funded by the European Union, Horizon Europe Funding Programme for Research and Innovation under grant agreement number: 101136548. ObsSea4Clim contribution no. 68.

Conflict of interest

All the authors declare no financial or non-financial competing interests.

Author contributions

Lionel D Swan 0009-0005-7492-9669
Conceptualization (equal), Formal analysis (lead), Visualization (lead), Writing – original draft (lead), Writing – review & editing (equal)

Samantha Hallam 0000-0003-3418-2554
Conceptualization (equal), Supervision (lead), Writing – original draft (supporting), Writing – review & editing (equal)

References

Acaps 2023 Madagascar–tropical cyclone Freddy exposure and vulnerabilities. anticipatory note (available at: www.acaps.org/fileadmin/Data_Product/Main_media/20230222_acaps_thematic_report_on_tropical_cyclone_freddy_exposure_and_vulnerabilities_in_madagascar_0.pdf) (Accessed 22nd February 2023)

Arora A, Rao S A, Chattopadhyay R, Goswami T, George G and Sabeerali C T 2016 Role of Indian Ocean SST variability on the recent global warming hiatus *Glob. Planet. Change* **143** 21–30

Ash K D and Matyas C J 2010 The influences of ENSO and the subtropical Indian Ocean dipole on tropical cyclone trajectories in the southwest Indian Ocean *Int. J. Climatol.* **32** 41–56

Astier N, Plu M and Claud C 2015 Associations between tropical cyclone activity in the southwest Indian Ocean and El Nino southern oscillation *Atmos. Sci. Lett.* **16** 506–11

Barcikowska M, Feser F and Storch H V 2012 Usability of best track data in climate statistics in the Western North Pacific. *Mon. Wea. Rev.* **140** 2818–30

Barrett B and Leslie L M 2009 Links between tropical cyclone activity and Madden–Julian oscillation phase in the North Atlantic and Northeast Pacific Basins *Mon. Wea. Rev.* **137** 727–44

Behringer D W and Xue Y 2004 Evaluation of the global ocean data assimilation system at NCEP: the Pacific Ocean *Eighth Symp. on Integrated Observing and Assimilation Systems for Atmosphere, Oceans, and Land Surface, AMS 84th Annual Meeting* (Washington State Convention and Trade Center) pp 11–15

Bessafi M and Wheeler M C 2006 Modulation of South Indian Ocean tropical cyclones by the Madden–Julian oscillation and convectively coupled equatorial waves *Mon. Wea. Rev.* **134** 638–56

Bousquet O *et al* 2021 Impact of tropical cyclones on inhabited Areas of the SWIO basin at present and future Horizons. Part 1: overview and observing component of the research project RENOVRISK-CYCLONE *Atmosphere* **12** 544

Bureau of Meteorology 2026 Tropical monitoring and outlooks. Madden-Julian Oscillation (MJO) (available at: www.bom.gov.au/climate/mjo/)

Burns J M, Subrahmanyam B, Nyadjro E S and Murty V S N 2016 Tropical cyclone activity over the southwest tropical Indian Ocean *J. Geophys. Res. Ocean* **121** 6389–402

Chand S S *et al* 2022 Declining tropical cyclone frequency under global warming *Nat. Clim. Change* **12** 655–61

Chand S S and Walsh K J E 2010 The influence of the Madden–Julian oscillation on tropical cyclone activity in the Fiji Region *J. Clim.* **23** 868–86

Cheung K K W, Jiang N, Liu K S and Chang L T-C 2015 Interdecadal shift of intense tropical cyclone activity in the southern hemisphere *Int. J. Climatol.* **35** 1519

Crnivec N, Smith R K and Kilroy G 2016 Dependence of tropical cyclone intensification rate on sea-surface temperature *Q. J. R. Meteorol. Soc.* **142** 1618–27

Doocy S, Dick ADaniels A and Kirsch TD 2013 The human impact of tropical cyclones: a historical review of events 1980–2009 and systematic literature review *PLoS Curr. Disasters* **5** 1–38

Elsner J B, Kossin J P and Jagger T H 2008 The increasing intensity of the strongest tropical cyclones *Nature* **455** 92–95

Emanuel K 1999 Thermodynamic control of hurricane intensity *Nature* **401** 665–9

Fitchett J M and Grab S W 2014 A 66-year tropical cyclone record for south-east Africa: temporal trends in a global context *Int. J. Climatol.* **34** 3604–15

Gahtan J, Knapp K R, Carl III J S, Diamond H J, Kossin J P and Kruk S 2024 International Best Track Archive for Climate Stewardship (IBTrACS) Project, Version 4.01. [Southern Indian] (NOAA National Centers for Environmental Information) (https://doi.org/10.25921/82ty-9e16) (Accessed 18 July 2025)

Goldenberg S B and Shapiro L J 1996 Physical mechanisms for the association of El Niño and West African rainfall with Atlantic Major Hurricane activity *J. Clim.* **9** 1169–87

Gray W M 1968 Global view of the origin of tropical disturbances and storms *Mon. Wea. Rev.* **96** 669–700

Hall J D, Matthews A J and Karoly D J 2001 The modulation of tropical cyclone activity in the Australian Region by the Madden–Julian Oscillation *Mon. Weather Rev.* **129** 2970–82

Hallam S 2021 The impact of Atlantic Ocean variability on North Atlantic storminess and the Northern Hemisphere Jet Stream *Thesis for the degree of Doctor of Philosophy* University of Southampton (available at: https://eprints.soton.ac.uk/id/eprint/451502/1/Final_thesis.pdf)

Hallam S, Guishard M, Josey S A, Hyder P and Hirschi J 2021 Increasing tropical cyclone intensity and potential intensity in the subtropical Atlantic around Bermuda from an ocean heat content perspective 1955–2019 *Environ. Res. Lett.* **16** 034052

Hallam S, Hallam JAird R, Campbell D, McCarthy GD and Guishard M 2026 Increasing hurricane intensity in the Caribbean is linked to rising subsurface ocean temperatures *Preprint* (https://doi.org/10.21203/rs.3.rs-8680876/v1)

Harper B A, Kepert J D and Ginger J D 2010 Guidelines for converting between various wind averaging periods in tropical cyclone conditions *WMO* (available at: www.systemsengineeringaustralia.com.au/download/WMO_TC_Wind_Averaging_27_Aug_2010.pdf)

Ho C, Kim J, Jeong J, Kim H-S and Chen D 2006 Variation of tropical cyclone activity in the South Indian Ocean: El Niño–Southern Oscillation and Madden-Julian Oscillation effects *J. Geophys. Res. Atmos.* **111** n/a

Huang B, Thorne P W and Banzon V F 2017 NOAA extended reconstructed sea surface temperature (ERSST), Version 5 (NOAA National Centers for Environmental Information (available at: www.ncei.noaa.gov/access/metadata/landing-page/bin/iso?id=gov.noaa.ncdc:C00927) (Accesed 18 July 2025)
Huang P, Lu Y and Zhou S 2018 An objective method for determining ocean mixed layer depth with applications to WOCE data *J. Atmos. Ocean. Technol.* **35** 441–58
Kiladis G N, Dias J, Straub K H, Wheeler M C, Tulich S N, Kikuchi K, Weickmann K M and Ventrice M J 2014 A comparison of OLR and circulation based indices for tracking the MJO *Mon. Weather Rev.* **142** 1697–715
Kim J, Ho C, Kim H, Sui C-H and Park S K 2008 Systematic variation of summertime tropical cyclone activity in the Western North Pacific in relation to the Madden–Julian Oscillation *J. Clim.* **21** 1171–91
Klotzbach P J 2014 The Madden–Julian Oscillation's impacts on worldwide tropical cyclone activity *J. Clim.* **27** 2317–30
Klotzbach P J, Wood K M, Schreck C J, Bowen S G, Patricola C M and Bell M M 2022 Trends in global tropical cyclone activity: 1990–2021 *Geophys. Res. Lett.* **49** e2021GL095774
Knaff J A, Brown D P, Courtney J, Gallina G M and Beven J L 2010 An evaluation of dvorak technique–based tropical cyclone intensity estimates *Wea. Forecasting* **25** 1362–79
Knapp K R, Kruk M C, Levinson D H, Diamond H J and Neumann C J 2010 the international best track archive for climate stewardship (IBTrACS): unifying tropical cyclone best track data *Bull. Am. Meteorol. Soc.* **91** 363–76
Kossin J P, Olander T L and Knapp K R 2013 Trend Analysis with a new global record of tropical cyclone intensity *J. Clim.* **26** 9960–76
Leroux M, Bonnardot F, Somot S, Alias A, Kotomangazafy S, Ridhoine A-O S, Veerabadren P and Amélie V 2024 Developing climate services for vulnerable islands in the Southwest Indian Ocean: a combined statistical and dynamical CMIP6 downscaling approach for climate change assessment *Clim. Serv.* **34** 100491
Leroux M, Meister JMekies D, Dorla AL and Caroff P. A 2018 A climatology of southwest Indian Ocean tropical systems: their number, tracks, impacts, sizes, empirical maximum potential intensity and intensity changes *AMS J. Appl. Meteorol. Climatol.* **57** 1021–41
Li J and Su J 2021 Sustained decadal warming phase in the southwestern Indian Ocean since the mid-1990s *J. Meteorol. Res.* **35** 258–70
Lin I-I, Black P, Price J F, Yang C-Y, Chen S S, Lien C-C, Harr P, Chi N-H, Wu C-C and D'Asaro E A 2013 An ocean coupling potential intensity index for tropical cyclones *Geophys. Res. Lett.* **40** 1878–82
Lin I *et al* 2020 ENSO and Tropical Cyclones *El Nino Southern Oscillation in a Changing Climate* (*Geophysical Monograph Series*) (American Geophysical Union) pp 377–408 Ch 17
Mahala B K, Nayak B K and Mohanty P K 2015 Impacts of ENSO and IOD on tropical cyclone activity in the Bay of Bengal *Nat. Hazards* **75** 1105–25
Maue R N 2011 Recent historically low global tropical cyclone frequency *Geophys. Res. Lett.* **38** n/a
Mavume A F, Rydberg L, Rouault M and Lutjeharms J R 2009 Climatology and landfall of tropical cyclones in the south-west Indian Ocean *West. Indian Ocean J. Mar. Sci.* **8** n/a
McTaggart-Cowan R, Galarneau T J Jr, Bosart L F, Moore R W and Martius O 2013 A global climatology of baroclinically influenced tropical cyclogenesis* American Meteorological Society *Mon. Weather Rev.* **141** 1963–89
Miller B I 1958 On the maximum intensity of hurricanes *AMS J. Atmos. Sci.* **15** 184–95
Murakami H, Hsu P, Arakawa O and Li T 2014 Influence of model biases on projected future changes in tropical cyclone frequency of occurrence *J. Clim.* **27** 2159–81
NOAA 2025a Southern Oscillation Index (SOI) (available at: www.ncei.noaa.gov/access/monitoring/enso/soi)
NOAA 2025b Niño regions sea surface temperatures (available at: www.ncei.noaa.gov/access/monitoring/enso/sst)
NOAA 2026a Daily MJO index time series from 1979 (available at: https://psl.noaa.gov/mjo/mjoindex/)
NOAA 2026b MJO phase plots. MJO phases using OLR (available at: https://psl.noaa.gov/mjo/phasetool/)
Office M n.d. Past tropical cyclones—South-West Indian tropical cyclone activity (available at: www.metoffice.gov.uk/research/weather/tropical-cyclones/observations/southwestindian)
Pillay M T and Fitchett J M 2019 Tropical cyclone landfalls south of the tropic of Capricorn, southwest Indian Ocean *Clim. Res.* **79** 23–37
Python 2026 About Python (available at: www.python.org/about/)
R 2021 What is R? (available at: www.r-project.org/about.html)
Rakotoarimanana Z M H, Rakotoarimanana Z H, Pandin M G R and Christrijogo Sumartono W 2022 Analysis of tropical cyclones 2000–2020 in Madagascar *Disaster Adv.* **15** 13–20
Republique de Madagascar, 2014 Strategie Nationale De Gestion Des Risques Et Des Catastrophes 2016–2020 (available at: https://drmims.sadc.int/sites/default/files/document/2020-03/2014_National_Risk_Disaster_Management_Strategy_2016-20.pdf)
Semgomba D S, Deng J and King-Uza P H 2025 Interannual relationship between ENSO and Tropical cyclone Genesis over the southwest Indian Ocean and its modulation by the interdecadal pacific oscillation *J. Geosci. Environ. Prot.* **13** 29–46
Strachan J, Vidale P L, Hodges K, Roberts M and Demory M-E 2013 Investigating global tropical cyclone activity with a hierarchy of AGCMs: the role of model resolution *J. Clim.* **26** 133–52
Terry J P, Kim I and Jolivet S 2013 Sinuosity of tropical cyclone tracks in the south west Indian Ocean: spatio-temporal patterns and relationships with fundamental storm attributes *Appl. Geogr.* **45** 29–40
Tory K J and Dare R A 2015 Sea Surface temperature threshold for tropical cyclone formation *J. Clim.* **28** 8171–83
Tory K J and Frank W M 2010 Tropical cyclone formation *World Scientific Series on Asia-Pacific Weather and Climate, Global Perspectives on Tropical Cyclones* pp 55–91
Vatcheva K P, Lee MMcCormick J B and Rahbar MH 2016 Multicollinearity in regression analyses conducted in epidemiologic studies *Epidemiology* **6** 227
Vecchi G A and Soden B J 2007 Effect of remote sea surface temperature change on tropical cyclone potential intensity *Nature* **450** 1066–70
Vialard J, Foltz G R, McPhaden M J, Duvel J P and de Boyer Montégut C 2008 Strong Indian Ocean sea surface temperature signals associated with the Madden-Julian Oscillation in late 2007 and early 2008 *Geophys. Res. Lett.* **35** n/a
Wahiduzzaman M, Ali M A, Cheung K, Luo J-J, Shaolei T, Bhaskaran P K, Yuan C, Bilal M, Qiu Z and Almazroui M 2022 Impacts of Aerosols and climate modes on tropical cyclone frequency over the North Indian Ocean: a statistical link approach *J. Clim.* **35** 2549–64
Walsh K J E *et al* 2015 Tropical cyclone and climate change *WIREs Clim. Change* **7** 65–89
Wang B and Rui H 1990 Synoptic climatology of transient tropical intraseasonal convection anomalies: 1975–1985 *Meteorl. Atmos. Phys.* **44** 43–61

Wang Y and Wu C C 2004 Current understanding of tropical cyclone structure and intensity changes—a review *Meteorol. Atmos. Phys.* **87** 257–78

Webster P J, Holland G J, Curry J A and Chang H-R 2005 Changes in tropical cyclone number, duration, and intensity in a warming environment *Science* **309** 1844–6

Willis J K, Fournier S and Marlis K 2025 NASA-SSH IOD sea surface height anomaly indicator Ver. 1. PO.DAAC (Accessed 18 July 2025) (https://doi.org/10.5067/NSIND-IODV1)

WMO 2017 Global guide to tropical cyclone forecasting. No. 1194 (available at: https://cyclone.wmo.int/pdf/Global-Guide-to-Tropical-Cyclone-Forecasting.pdf)

Wu L, Wang R and Feng X 2018 Dominant role of the ocean mixed layer depth in the increased proportion of intense typhoons during 1980–2015 *Earth's Future* **6** 1518–27

Yan C, Hong-Ming Y, Yun T, YANG K-L and Wang M-Q 2023 The relationship between Indian Ocean SST and tropical cyclone genesis frequency over north Indian Ocean in May *J. Trop. Meteorol.* **29** 359–69

Yoshida K, Sugi M, Mizuta R, Murakami H and Ishii M 2017 Future changes in tropical cyclone activity in high-resolution large-ensemble simulations *Geophys. Res. Lett.* **44** 9910–7

Yuan J and Cao J 2012 North Indian Ocean tropical cyclone activities influenced by the Indian Ocean dipole mode *Sci. China Earth Sci.* **56** 855–65

Zhang Y, Han KSun Y, Lin Y, Zhai P, Guo X and Zhong W 2024 Impact of ocean mixed layer depth on tropical cyclone characteristics: a numerical investigation *Front. Mar. Sci. Sec. Phys. Oceanogr.* **11** 1395492

Zhao M, Held I M, Lin S and Vecchi G A 2009 Simulations of global hurricane climatology, interannual variability, and response to global warming using a 50-km resolution GCM *J. Clim.* **22** 6653–78